Clinical Progress

Cell Stem Cell

Human ESC-Derived Dopamine Neurons Show Similar Preclinical Efficacy and Potency to Fetal Neurons when Grafted in a Rat Model of Parkinson's Disease

Graphical Abstract

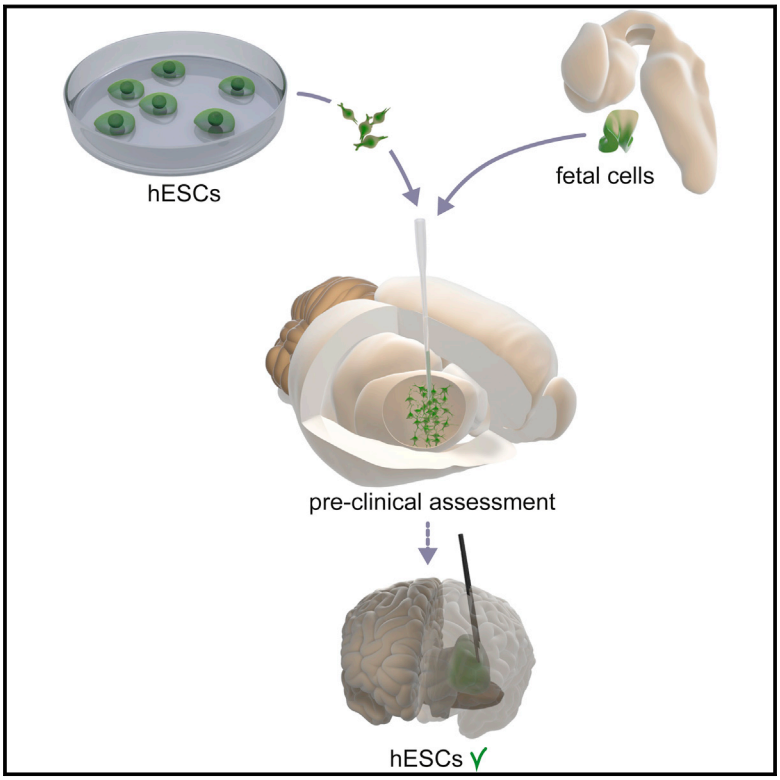

Highlights

Transplants of hESC-DA survive long term and restore DA neurotransmission in vivo

The functional potency of hESC-DA is similar to human fetal midbrain DA neurons

hESC-DA are capable of long-distance, target-specific innervation of the host brain

The axonal outgrowth capacity of hESC-DA meets the requirements for use in humans

Authors

Shane Grealish, Elsa Diguet, ..., Anders Björklund, Malin Parmar

Correspondence

shane.grealish@med.lu.se (S.G.), malin.parmar@med.lu.se (M.P.)

In Brief

Grealish et al. provide preclinical evidence that hESC-derived dopamine neurons are functionally equivalent to those derived from fetal tissue, supporting continued development of hESC-derived cells as a clinical approach for the treatment of Parkinson's disease.

Grealish et al., 2014, Cell Stem Cell 15, 653–665
November 6, 2014 ©2014 The Authors
http://dx.doi.org/10.1016/j.stem.2014.09.017

Cell Stem Cell
Clinical Progress

Human ESC-Derived Dopamine Neurons Show Similar Preclinical Efficacy and Potency to Fetal Neurons when Grafted in a Rat Model of Parkinson's Disease

Shane Grealish,[1,2,*] Elsa Diguet,[3] Agnete Kirkeby,[1,2] Bengt Mattsson,[1] Andreas Heuer,[1,2] Yann Bramoulle,[3] Nadja Van Camp,[3] Anselme L. Perrier,[4,5] Philippe Hantraye,[3] Anders Björklund,[1] and Malin Parmar[1,2,*]
[1]Developmental and Regenerative Neurobiology, Department of Experimental Medical Science, Wallenberg Neuroscience Center, Lund University, 22184 Lund, Sweden
[2]Lund Stem Cell Center, Lund University, 22184 Lund, Sweden
[3]Molecular Imaging Research Centre (MIRCen), Commissariat à l'Energie Atomique (CEA), 92264 Fontenay-aux-Roses, France
[4]Inserm U861, I-Stem, AFM, 91030 Evry Cedex, France
[5]UEVE U861, I-Stem, AFM, 91030 Evry Cedex, France
*Correspondence: shane.grealish@med.lu.se (S.G.), malin.parmar@med.lu.se (M.P.)
http://dx.doi.org/10.1016/j.stem.2014.09.017

SUMMARY

Considerable progress has been made in generating fully functional and transplantable dopamine neurons from human embryonic stem cells (hESCs). Before these cells can be used for cell replacement therapy in Parkinson's disease (PD), it is important to verify their functional properties and efficacy in animal models. Here we provide a comprehensive preclinical assessment of hESC-derived midbrain dopamine neurons in a rat model of PD. We show long-term survival and functionality using clinically relevant MRI and PET imaging techniques and demonstrate efficacy in restoration of motor function with a potency comparable to that seen with human fetal dopamine neurons. Furthermore, we show that hESC-derived dopamine neurons can project sufficiently long distances for use in humans, fully regenerate midbrain-to-forebrain projections, and innervate correct target structures. This provides strong preclinical support for clinical translation of hESC-derived dopamine neurons using approaches similar to those established with fetal cells for the treatment of Parkinson's disease.

INTRODUCTION

Cell replacement therapy in Parkinson's disease (PD) is based on the premise that transplanted midbrain dopamine (DA) neurons can restore dopaminergic neurotransmission when transplanted to the DA-depleted striatum, providing a functionally efficient substitute for the neurons that are lost in the disease. Clinical trials using cells derived from human fetal ventral mesencephalon (VM) have shown that transplanted DA neurons can functionally reinnervate the denervated striatum, restore DA release, and at least in some PD patients, provide substantial long-term clinical improvement (Barker et al., 2013; Kefalopoulou et al., 2014). However, the use of tissue from aborted human embryos presents several ethical and logistical issues that hamper the effective translation of fetal tissue transplantation as a realistic therapeutic option.

In order to move to large-scale clinical applications, a readily available, renewable, and bankable source of cells with the potential to differentiate into fully functional DA neurons after transplantation is an absolute requirement. Among the different stem cell sources available, human pluripotent stem cells, in particular human embryonic stem cells (hESCs), have advanced the furthest (Lindvall and Kokaia, 2009; Barker, 2014). Using protocols entirely based on extrinsic patterning cues that mimic fetal midbrain development, it is now possible to generate DA neurons with an authentic midbrain phenotype from human pluripotent stem cells that survive transplantation and that can restore motor deficits in animal models of PD (Doi et al., 2014; Kirkeby et al., 2012a; Kriks et al., 2011).

However, a number of crucial issues need to be addressed in preclinical studies before these cells can be considered for clinical use: it is important to verify that their functional efficacy is robust, reproducible, and stable over significant time periods; that the transplanted cells have the capacity to grow axons and reinnervate the DA-denervated host striatum over distances that are relevant for the size of the human brain; and that they function with equal potency to human fetal VM DA neurons that have previously been used in clinical trials (Barker, 2014).

Here we have performed a rigorous preclinical assessment of long-term in vivo functionality and axonal outgrowth capacity of hESC-derived midbrain DA neurons, critical for their translation to the clinic. We show long-term survival and functionality using clinically relevant MRI and positron emission tomography (PET) imaging techniques and efficacy in restoration of motor function that is comparable to that seen with human fetal cells. Importantly, we provide a direct comparison of human DA neurons sourced from either hESCs or fetal VM and show that hESC-derived neurons, like their fetal counterparts, can project over long distances in the lesioned adult rodent brain and regenerate axonal projections with cell-type specific innervation of correct

target structures. These data represent an important milestone in the preclinical assessment of hESC-derived DA neurons and provide essential support for their usefulness in cell replacement therapy for PD.

RESULTS

Long-Term Survival and Restoration of Dopaminergic Neurotransmission by hESC-DA Neurons

First, we wanted to assess long-term survival and function of grafted cells using methodologies that are used in the clinic. We therefore transplanted hESC-derived DA (hESC-DA) neurons to the striatum of 6-hydroxydopamine (6-OHDA) lesioned athymic, adult rats, allowing for long-term graft survival in the absence of immunosuppressive treatment. The grafted animals were followed up to 6 months after transplantation, the point at which grafts of fetal VM in patients start to become functional (Piccini et al., 2000). T2-weighed MRI imaging showed surviving transplants that increased in volume from 1 to 5 months post-transplantation, indicating initial proliferation and subsequent maturation of the transplanted cells (Figure S1A available online), as previously described for transplants of proliferative midbrain progenitors (Kirkeby et al., 2012a). MR spectroscopy investigation 5 months postgrafting revealed a high *N*-acetylaspartic acid content within the transplanted area, indicative of a neuron-rich graft (Figures S1B and S1C). Pretransplantation, the rats were assessed for deficits in striatal dopaminergic neurotransmission by PET, using ^{18}F-fallypride as a measure of D_2/D_3-receptor occupancy (Moon et al., 2010) and ^{18}F-LBT999 as a tracer for the dopamine transporter (DAT) (Dollé et al., 2007) (Figure 1A). In the 6-OHDA-lesioned DA-denervated striatum ^{18}F-fallypride binding was significantly increased, as compared with the intact hemisphere, signifying a pronounced reduction in DA release. After grafting, ^{18}F-fallypride binding was normalized to intact levels as assessed 5 months posttransplantation, indicative of active DA release from the transplanted hESC-DA neurons (Figures 1A and 1B). Similarly, the near-complete loss of DAT binding, using ^{18}F-LBT999, seen after 6-OHDA lesion was reversed to around 50% of normal (Figures 1A and 1C). ^{18}F-DPA714 binding was used to measure microglial activation (Kuhnast et al., 2012), and no increase was observed at 5 months postgrafting, relative to the nontransplanted side (Figure 1A).

Histological Analysis and Innervation Capacity of hESC-DA Neurons after Intrastriatal Transplantation

Histological analysis confirmed the imaging data, showing neuron-rich transplants and revealing grafts rich in DA neurons, expressing both tyrosine hydroxylase (TH) and dopamine transporter (DAT), in the absence of a notable active microglial (Iba1$^+$) response, overgrowths, or necrotic areas (Figures S2A–S2C). To assess graft-derived axonal outgrowth we made use of an antibody specific for human neural cell adhesion molecule (hNCAM) (Figures 1D–1G), allowing selective and highly sensitive visualization of the grafted neurons and their projections. Dense hNCAM$^+$ innervation was observed throughout the caudate-putamen, including the dorsolateral striatum, which derives its innervation exclusively from the A9 neurons of the substantia nigra (SN) (Figure 1D). Similar innervation was also observed in other forebrain DA target areas outside the caudate-putamen, such as nucleus accumbens (NAc) (Figure 1E), olfactory tubercle (Figure 1D), and the perirhinal and prelimbic cortices (Figures 1F and 1G), which are essential targets for the A10 neuronal subtype, residing in the ventral tegmental area (VTA) (Figures S2D and S2E).

Taken together, these data prove the ability of hESC-DA neurons to provide extensive reinnervation of the host striatum and begin to restore DAergic neurotransmission 5 months posttransplantation, using clinically relevant methods to assess graft function, in the absence of significant adverse events. This is in line with previous clinical observations using human fetal VM grafted to patients, where progressive recovery of DA neurotransmission starts at 6 months, reflecting the gradual maturation of the transplanted cells (Piccini et al., 1999, 2000).

Functional Potency Assessment of hESC-DA Neurons Grafted to the Striatum

We and others have previously shown that hESC-DA neurons can release DA in vivo (Kirkeby et al., 2012a) and restore a number of motor deficits in 6-OHDA rodent models of PD when assessed 16–18 weeks after grafting (Kirkeby et al., 2012a; Kriks et al., 2011). However, these transplants contained 15,000–18,000 hESC-derived DA neurons, and the high cell number makes it difficult to estimate the efficacy of the cells (Barker, 2014). In previous preclinical and experimental studies using grafts of human fetal VM, it has been shown that normalization of amphetamine-induced rotation after intrastriatal transplantation can be achieved with an average number of 1,200 surviving TH$^+$ neurons (Brundin et al., 1986). On the basis of this information, we performed a potency experiment designed to determine the minimal number of hESC-DA neurons capable of inducing functional recovery in the amphetamine-induced rotation test. We transplanted 6-OHDA lesioned rats, aiming for at least a 10-fold lower number of hESC-DA than the grafts functionally assessed in earlier studies (Kirkeby et al., 2012a; Kriks et al., 2011). The rats were pretested to confirm the completeness of the lesion and immunosuppressed with daily injections of ciclosporin for 18 weeks. At this time point, the rats showed a significant recovery in amphetamine-induced rotation (Figure 2A: $t_4 = 6.76$, $p < 0.01$; $n = 5$), despite a much lower number of TH$^+$ neurons in the grafts (Figures 2B and 2C). Quantifications showed that the average number of surviving TH$^+$ neurons was 986 ± 333 per rat ($n = 5$). Two of the rats had less than 500 surviving hESC-DA neurons and yet showed a complete reduction in rotational bias (Figure 2B). Within TRANSERUO, a EU-funded research consortium formed to develop an efficacious and safe treatment methodology for PD using fetal cell based treatments (http://www.transeuro.org.uk), research groups including our own have optimized and standardized tissue preparation protocols across several centers throughout Europe. A recent report with cells prepared using this protocol show that a significant reduction in amphetamine-induced rotation could be achieved with transplants of human fetal VM with as few 657 ± 199 surviving TH$^+$ neurons (Rath et al., 2013). These results indicate that the functional potency of grafted hESC-DA neurons is on par with that of human DA neurons obtained from fetal VM (Brundin et al., 1986; Rath et al., 2013).

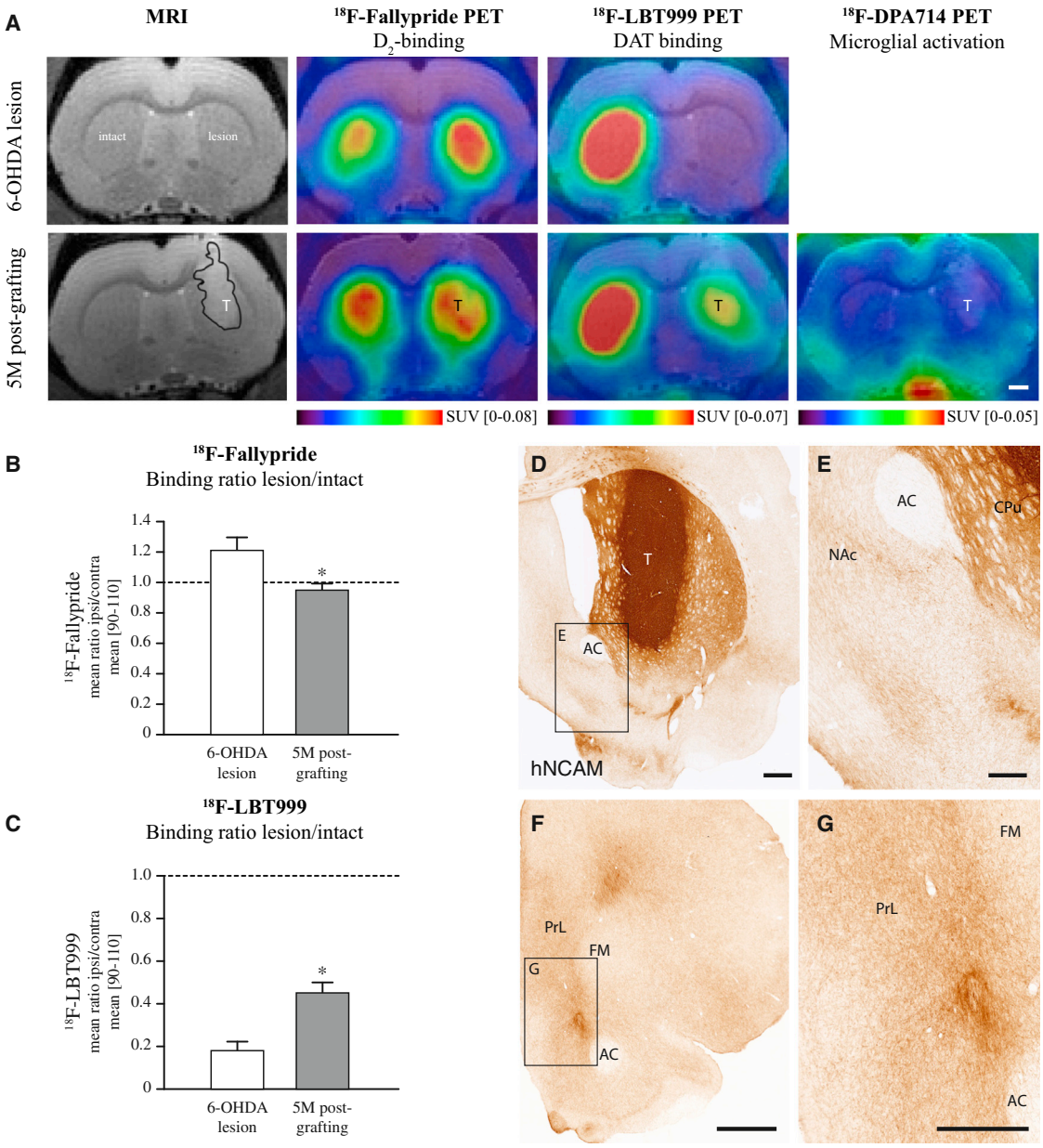

Figure 1. Functional Imaging of Long-Term Surviving Intrastriatal Transplants of hESC-DA Neurons

(A) MRI and PET scans for ^{18}F-fallypride, ^{18}F-LBT999 after 6-OHDA lesion, show an increase in binding of ^{18}F-fallypride (n = 6) on the side of lesion indicating an impaired DA release, confirmed by a loss of ^{18}F-LBT999 (n = 7) binding due to loss of DAT binding sites. At 5 months posttransplantation both ^{18}F-fallypride (n = 11) and ^{18}F-LBT999 (n = 14) binding are restored toward normal, indicative of a graft rich in functional DA neurons, in the absence of any detectable microglial response, as assessed with ^{18}F-DPA714 (n = 13).

(B) Quantitative measurements of binding ratios between intact and lesioned striatum revealed an increased binding potential of ^{18}F-fallypride in the 6-OHDA denervated striatum, which was normalized to intact levels 5 months posttransplantation of hESC-DA neurons.

(C) A 6-OHDA lesion resulted in a near complete loss of ^{18}F-LBT999 binding due to the loss of DAT-expressing dopaminergic terminals, which was restored toward normal posttransplantation.

(D and E) Immunohistochemistry of hNCAM revealed neuron-rich grafts of hESC-DA neurons 6 months posttransplantation, providing extensive innervation of the host CPu and surrounding extrastriatal dopaminergic targets, such as NAc.

(F and G) Away from the graft core, widespread innervation by human axons was found in known DA target structures within the prefrontal cortex.

See also Figure S1. AC, anterior commissure; CPu, caudate-putamen unit; FM, forceps minor; NAc, nucleus accumbens; PrL, prelimbic cortex; T, transplant. In (B) and (C), data are represented as mean ± SEM. *p < 0.01. In (A), (D), and (F), scale bars represent 1 mm. In (E) and (G), scale bars represent 0.5 mm.

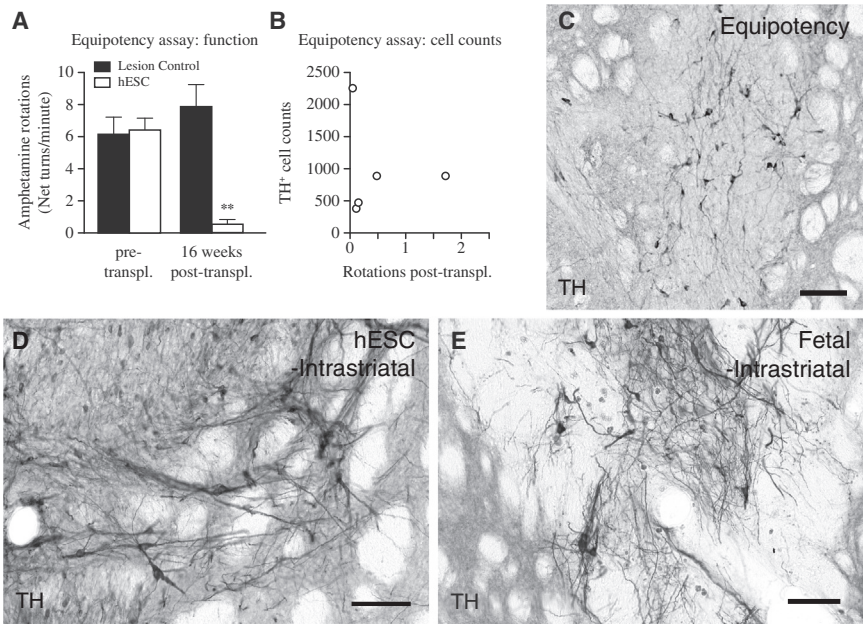

Figure 2. Functional Equipotency of Intrastriatal Transplanted hESC-DA Neurons and Comparable Morphology to Grafts of Fetal VM-Derived DA Neurons

(A) 6-hydroxydopamine lesioned rats displayed a strong unilateral rotational bias upon administration of amphetamine, which was significantly normalized 16 weeks after intrastriatal transplantation of hESC-DA neurons (white bars, n = 5), whereas lesion controls (black bars, n = 6), not receiving any transplant, showed no significant changes when monitored in parallel.

(B) Estimation of the number of surviving TH^+ neurons within the graft revealed a relatively low number that gave rise to graft-mediated functional recovery.

(C) Histological analysis revealed grafts with sparse numbers of TH^+ neurons dispersed throughout.

(D and E)When comparing transplants of hESC-derived (D) and fetal-derived (E) DA neurons 6 months posttransplantation, both groups revealed grafts rich in DA neurons that are indistinguishable on a gross morphological level.

See also Figure S2. TH, tyrosine hydroxylase. In (A), data are represented as mean ± SEM. **$p < 0.01$. In (C)–(E), scale bars represent 100 μm.

Histological Comparison of DA Neurons Sourced from Human Fetal VM and hESCs after Intrastriatal Transplantation

We next performed a direct histological comparison between hESC-DA neurons and authentic human fetal DA neurons prepared according to Rath et al. (2013), grafted in parallel, in order to validate the morphology, maturation, and phenotypic properties of the transplanted DA neurons (Figures 2D and 2E). In this analysis, we observed the presence of TH^+ neurons with two distinct morphologies in the hESC-grafted animals (Mendez et al., 2005; Thompson et al., 2005): A9-like nigral neurons characterized by large angular somata and A10-like VTA neurons with small, round somata (Figure 3A). The morphology of the hESC-derived neurons was identical to that observed with intrastriatal transplants of fetal VM when analyzed at 6 months posttransplantation (Figure 3C) and consistent with graft appearance from previous postmortem reports from transplanted PD patients (Mendez et al., 2005). When staining the cells for markers commonly used to distinguish between SN (A9) and VTA (A10) neurons, TH^+ neurons expressing GIRK2 (A9), Calbindin (A10), or both markers were readily detected (Figures 3B and 3D). Quantifications showed that $TH^+/GIRK2^+$ neurons were the most abundant subtype in both hESC-derived and fetal grafts (Figure 3I) and that the proportion was similar in both hESC- and fetal-derived grafts (Figure 3J). Taken together, this analysis shows that hESC-DA neurons are indistinguishable from their fetal counterparts on the basis of graft appearance, morphology, and marker expression 6 months after grafting and that the hESC-derived grafts are rich in both A9-like and A10-like DA neurons.

Long-Distance Axonal Outgrowth of hESC-Derived Neurons after Transplantation into the Substantia Nigra

When assessing the cells for their suitability to be used in clinical trials, it is important to keep in mind that the human brain is a much larger structure than the rodent brain and that it is necessary for the transplanted cells to extend axons over long distances in order to sufficiently reinnervate the putamen in patients. We therefore sought to create an assay through which long-distance, target-specific outgrowth could be assessed in an adult rodent model of PD that would be predictive when translating to the larger human brain. Intrastriatal grafting, the standard used in preclinical and clinical studies, places the cells within their main target structure, thus making it difficult to assess the full innervation capacity of human cells when grafted to the rat brain. To investigate the ability of hESC-DA neurons to innervate specific structures across longer distances, we employed a homotopic grafting approach where we transplanted hESC-DA neurons into the lesioned SN, instead of the traditional ectopic placement in the striatum. Transplants of fetal VM served as an important reference to see if hESC-derived neurons could match their capacity for long-distance and target-specific innervation.

When grafted to the SN, both hESCs and fetal VM gave rise to grafts rich in TH^+ neurons expressing GIRK2 and Calbindin with morphologies indistinguishable from cells grafted to the striatum (compare Figures 3E–3H with Figures 3A–3D). In the majority of rats with fetal VM transplants (n = 7/8), we observed neuron-rich grafts, discretely placed within the host SN, extending large numbers of $hNCAM^+$ axons rostral along the medial forebrain bundle (MFB) and the adjacent nigrostriatal pathway, assembled in a well-defined and fasciculated tract (Figures 4A, 4G, 4I, S3A, and S3B). Rostral extending axonal bundles were seen to defasciculate and ramify within their terminal target fields, providing widespread innervation of specific host structures throughout the forebrain (Figure 4A), extending more than 10 mm from the graft core. $hNCAM^+$ terminal innervation was particularly dense in caudate-putamen (Figure 4C), NAc (Figure 4D), amygdala (Figure 4B), and perirhinal and anteromedial frontal cortices (Figures 4A and 4E).

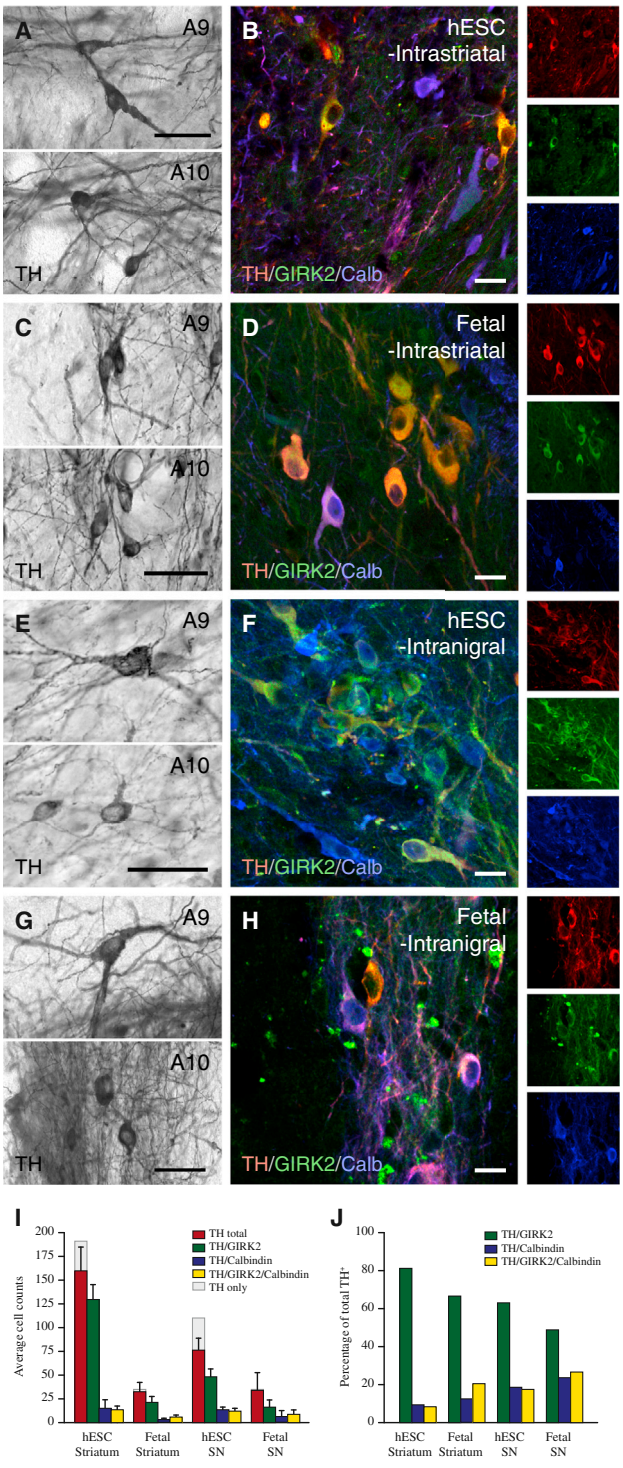

Figure 3. Comparison of A9 and A10 Midbrain DA Neuron Subtypes in Long-Term Grafts of hESC-DA Neurons and Human Fetal VM

(A) Upon close inspection, hESC-DA neurons gave rise to TH$^+$ dopaminergic neurons with an A9-like neuron morphology, characterized by large angular somas (upper panel), as well as A10-like neurons with small, round somas (lower panel).

(B) The presence of neurons coexpressing TH and GIRK2 (red and green) and TH and Calbindin (red and blue) indicates that both midbrain DA neuron subtypes, A9 and A10, were contained in grafts of hESC-derived neurons.

(C and D) Intrastriatal grafts of human fetal VM contained TH$^+$ dopaminergic neurons with A9 and A10 morphologies, coexpressing GIRK2 and/or Calbindin.

(E and F) Homotopic placement of hESC-DA neurons in SN resulted in large numbers of TH$^+$ dopaminergic neurons with mature A9 and A10 morphologies, confirmed by coexpression of TH with GIRK2 and Calbindin, respectively.

(G and H) Fetal VM tissue grafted to the SN displayed the same ability to generate transplants with dopaminergic neurons of A9 and A10 morphologies and protein expression (H).

(I and J) The number and proportion (J) of TH$^+$ neurons, coexpressing GIRK2, Calbindin, or both markers, was quantified in all groups (n = 3 per group).

Calb, Calbindin; GIRK2, G protein-regulated inward-rectifying potassium channel 2; TH, tyrosine hydroxylase. In (I) and (J), data are represented as mean ± SEM. In (A), (C), (E), and (G), scale bars represent 50 μm. In (B), (D), (F), and (H), scale bars represent 20 μm.

Notably, graft-derived hNCAM$^+$ glial cells were detected in the transplants derived from the 8-week-old fetus (Figures 4F and 4G), but not from the younger 5.5-week-old fetus (Figures 4H and 4I). In the grafts of 8-week fetal VM, the graft-derived glial cells could be traced along myelinated and nonmyelinated fiber tracts, accompanying the hNCAM$^+$ axons up to the level of the caudal caudate-putamen (Figure 4G), as described in previous xenografting studies (Gates et al., 1998; Isacson et al., 1995; Pundt et al., 1995). Despite the absence of graft-derived glia in the transplants of the younger embryo (Figure 4H), hNCAM$^+$ fiber outgrowth was comparable to grafts derived from older tissue (Figures S3B–S3G). This observation indicates that the extent and patterning of axonal outgrowth is largely independent of this glial population present within the transplant.

Six months posttransplantation we observed robust survival in all hESC grafted animals (n = 8/8), with no signs of overgrowth or necrosis, similar in morphology to the intrastriatal grafts of hESC-DA neurons described above (Figures 1, 2D, and S2A–S2C). As observed with intranigral transplants of fetal VM, large numbers of hNCAM$^+$ fibers projected rostral along the MFB and the adjacent nigrostriatal pathway (Figures 5A, 5F, S4A, and S4B). The axons extending along the MFB continued a distance more than 10 mm from the graft core and gave rise to dense terminal networks in amygdala (Figure 5B); dorsolateral striatum (Figure 5C) and piriform cortex; ventral striatum, including NAc (Figure 5D); olfactory tubercle; lateral septum; and large parts of the frontal lobe (Figures 5A, 5E, and 5G). hNCAM$^+$ cells with a glial morphology were not detected in any of the hESC-grafted rats, consistent with our hypothesis that they are not essential for extensive axonal outgrowth.

Subtype Identity and Target-Specific Innervation of hESC-DA Neurons after Transplantation into the Substantia Nigra

Although A9 and A10 midbrain DA neuron subtypes can be arbitrarily distinguished on the basis of morphology and GIRK2/Calbindin protein expression, true identification of the subtype is linked to the ability of the neurons to innervate their appropriate forebrain targets: the A9 preferentially innervating the caudate-putamen and A10 neurons innervating limbic and cortical areas, including ventral striatum and NAc. To determine the presence of authentic A9 or A10 subtypes in grafts of fetal VM and hESC-DA neurons, we performed quantitative fiber density measurements (Figures S5A and S5B) of human hNCAM$^+$ axons (Figure 6C) in

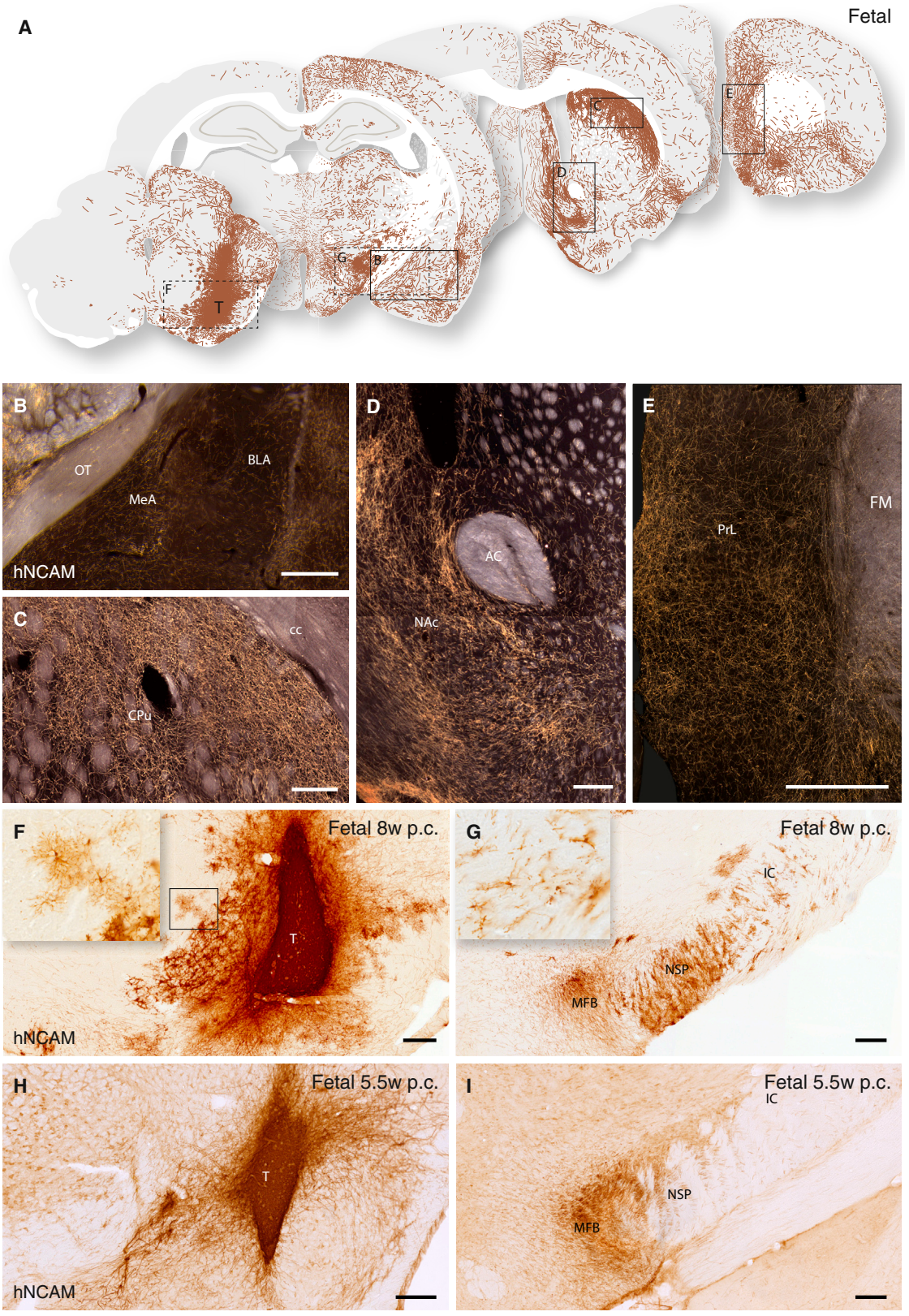

(legend on next page)

defined striatal areas (A9 targets), as well as limbic and cortical areas (A10 targets), as depicted in Figure S5C.We found that the number of axons projecting rostral was similar in the VM (2,169 ± 181; n = 3) and hESC (2,453 ± 774; n = 4) groups. Overall, the fiber density measurements showed that the midbrain-patterned hESCs exhibited the same A9/A10 target specificity and axonal outgrowth patterns as human fetal VM cells. Both fetal VM- and hESC-derived neurons innervated the caudate-putamen, which in the rat is targeted almost exclusively by A9 neurons, but that fetal VM tissue was more efficient at innervating the dorsolateral caudate-putamen (Figure 6A: dorsomedial, $t_{25} = 2.69$, $p < 0.01$; dorsolateral, $t_{25} = 4.38$, $p < 0.0001$; Medial, $t_{25} = 2.14$, $p < 0.05$). All A10-specific target structures were innervated at similar densities by fetal VM and hESCs, with the exception of the infralimbic cortex and septum, which received a more pronounced innervation from the hESC grafts (Figure 6B: ILC, $t_{25} = 5.99$, $p < 0.0001$; Sept, $t_{25} = 5.32$, $p < 0.0001$).

In order to identify the specific contribution from grafted DA neurons, we utilized immunofluorescence to detect human axons coexpressing TH and hNCAM (Figure 6F). Performing fiber density counts on double-positive fibers; we again found that fetal- and hESC-derived DA neurons demonstrated a similar propensity to innervate A9 and A10 specific striatal target structures (Figures 6D and 6E), although A9-specific innervation derived from fetal VM grafts was overall of higher density (Figure 6D: dorsomedial, $t_4 = 2.27$, $p < 0.05$; dorsolateral, $t_4 = 4.15$, $p < 0.01$).

In summary, midbrain-patterned hESCs exhibited the same remarkable ability as their fetal counterparts to extend axons over long distances and provide specific innervation of the relevant A9 and A10 host target structures. GIRK2 and Calbindin are commonly used as subtype markers for stem cell-derived DA neurons in vitro and after transplantation (Kirkeby et al., 2012a; Kriks et al., 2011; Ryan et al., 2013). However, we notice here that a high GIRK2$^+$ component (Figures 3I and 3J) does not directly translate to a strong innervation of the A9 target structures (Figures 6A and 6D). This observation is supported by the postmortem analysis of the adult human midbrain, which reveals that colocalization of TH and GIRK2 occurs in all DAergic neurons of the SN, but also in a substantial portion of DAergic neurons of the VTA (Reyes et al., 2012), thus calling for a more stringent analysis of A9 subtype of stem cell-derived DA neurons.

Expression of OTX2 Alters the Axonal Outgrowth Pattern of Transplants of hESC-Derived Neurons

Next, we sought to investigate if target-specific axonal outgrowth from hESC-DA neurons is a cell intrinsic property that can be regulated by transcriptional programming. Experiments in mice have established a major role for the transcription factor *Otx2* in the development of the midbrain DA progenitors. The expression of this transcription factor is maintained selectively in DA neurons with a mature A10 phenotype, where it acts to control the pattern of axonal outgrowth in forebrain structures (Chung et al., 2010, 2005; Di Salvio et al., 2010a, 2010b). We generated transgenic hESCs (*OTX2*-hESCs) using a lentiviral construct that expresses *OTX2* at physiologically relevant levels under the control of the PGK promoter and contains miRNA-292 target sequences to restrict expression to differentiated progeny (Sachdeva et al., 2010) (Figures S6A and S6B). We verified that the transgene did not disturb patterning toward a midbrain fate, as *OTX2*-hESCs gave rise to a similar number of LMX1A, FOXA2, and OTX2 expressing progenitors, as compared with wild-type (WT) hESCs (compare Figures S6D and S6E with Figures S4C and S4D). At a later time point in vitro, and consistent with the emergence of mature TH$^+$ neurons, OTX2 was downregulated in mature MAP2$^+$/TH$^+$ neurons from parental WT hESCs, but specifically maintained in differentiated *OTX2*-hESCs (Figures S6C and S6F). The *OTX2*-hESC-derived DA neuron progenitors were transplanted to the SN of 6-OHDA-lesioned athymic rats (n = 8). At 6 months, immunohistochemical analysis revealed a pronounced expression of OTX2 within the graft core at a level exceeding that observed in grafts of fetal VM and WT hESCs (Figures S6G–S6I). The *OTX2*-hESC grafts exhibited a similar axonal outgrowth pattern to the WT hESCs, with large numbers of hNCAM$^+$ axons extending rostral within the MFB (Figures 7A and 7B). However, the innervation derived from the *OTX2*-hESCs was restricted almost exclusively to A10 target structures, including NAc; ventral striatum; septum; amygdala; and antero-medial regions of the prefrontal cortex (Figures 7A–7E and S6K). Few, if any, hNCAM$^+$ fibers were observed in A9 target structures, such as dorsolateral caudate-putamen (Figures 7A and 7C). When quantifying the innervation of all measured A9 structures (dorsomedial, dorsolateral, medial, and central aspects of the caudate-putamen unit; Figure S5C), *OTX2*-hESCs displayed a reduced preference for innervating A9 target structures both when compared with grafts of the parental hESCs and with fetal-derived DA neurons (Figure 7H: $F_{(2,\ 105)} = 28.91$, $p < 0.0001$; difference confirmed using a Tukey's post hoc test, $p < 0.001$).

To exclude that this dramatic switch in target innervation was due to experimental variation or altered in vitro patterning, we replicated this experiment with a new cell differentiation and transplanted to immunocompetent rats under immunosuppression

Figure 4. Extent and Pattern of Axonal Outgrowth from Intranigral Transplants of Human Fetal VM 6 Months Posttransplantation

(A) Schematic overview of hNCAM$^+$ fibers from an intranigral transplant of fetal VM, innervating the host brain as visualized under dark-field illumination of DAB-developed sections (see Figure S3A).

(B–E) Transplants of fetal VM displayed a strong preference for innervating: amygdala (including MeA and BLA) (B); dorsolateral caudate-putamen (C); and nucleus accumbens, NAc (D). Graft-derived axons were found as far as 10 mm away from the graft core in areas of the prefrontal cortex (E).

(F–I) In bright-field illumination, the appearance of the 8-week (F) and 5.5-week (H) donor transplants and the associated outgrowth of hNCAM$^+$ axons in the MFB and the adjacent nigrostriatal pathway (G and I), including the presence of migrating hNCAM$^+$ graft-derived glial cells in the older donor transplants (Insets in F and G). See also Figure S3. AC, anterior commissure; BLA, basolateral amygdala; CPu, caudate-putamen; FM, forceps minor; IC, internal capsule; MeA, medial amygdaloid nucleus; MFB, medial forebrain bundle; NAc, nucleus accumbens; NSP, nigrostriatal pathway; p.c., postconception; PrL, prelimbic cortex; T, transplant. In (B), (D), (F), (G), (H), and (I), scale bars represent 0.2 mm. In (C) and (E), scale bars represent 0.5 mm.

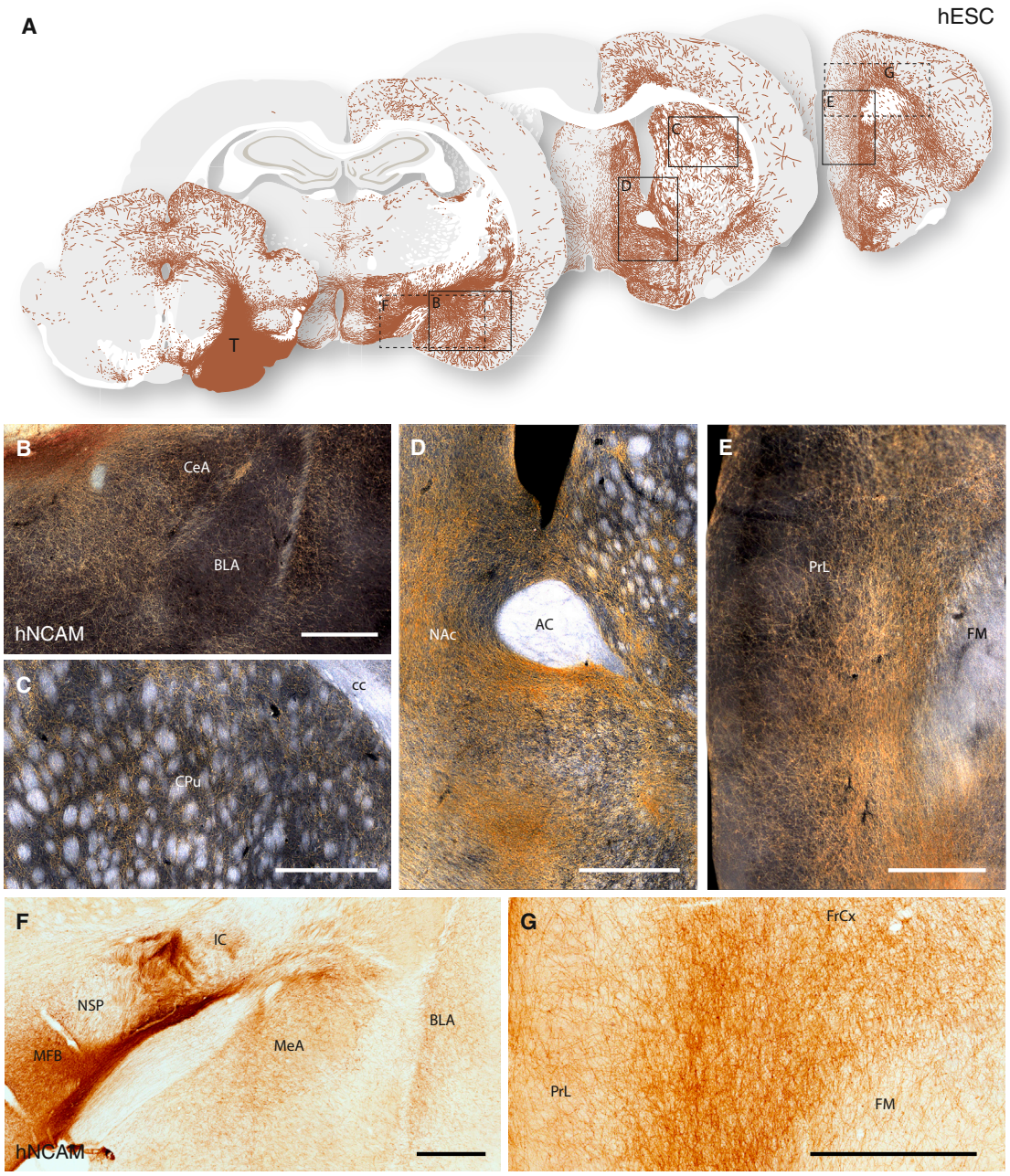

Figure 5. Overview of Neuronal Outgrowth of Intranigral Transplants of hESC-DA Neurons 6 Months after Transplantation

(A) Schematic overview of hNCAM$^+$ fiber outgrowth from an intranigral transplant of hESC-DA neurons, as visualized under dark-field illumination of DAB-developed sections (see Figure S4A).

(B–D) Higher magnification illustrates the hESC-derived innervation patterns of the amygdala (B), caudate-putamen (C), and NAc (D).

(E–G) hNCAM$^+$ fiber bundles were seen to extend rostral within the MFB and nigrostriatal pathway (E), and also within the myelinated white matter tracts of the internal capsule (F), over a distance of more than 10 mm from the graft core to innervate parts of the prefrontal cortex (E and G).

See also Figure S4. AC, anterior commissure; BLA, basolateral amygdala; CeA, Central Amygdaloid nucleus; CPu, caudate-putamen unit; FM, forceps minor; IC, internal capsule; MeA, medial amygdaloid nucleus; MFB, medial forebrain bundle; NAc, nucleus accumbens; NSP, nigrostriatal pathway; PrL, prelimbic cortex; T, transplant. In (B)–(G), scale bars represent 0.5 mm.

using daily injections of ciclosporin. In all animals (n = 7/7; 14-week survival), grafts of *OTX2*-hESCs were efficiently differentiated into mature TH$^+$ neurons (Figure S6J), and the identical pattern of A10-specific target innervation was observed (Figures 7F and 7G).

These findings provide evidence that target-specific outgrowth, attributed to a given midbrain DA neuron subtype, can be controlled and redirected in hESC-derived cell preparations, thus providing an opening for future efforts to enhance the fiber outgrowth to specific target nuclei.

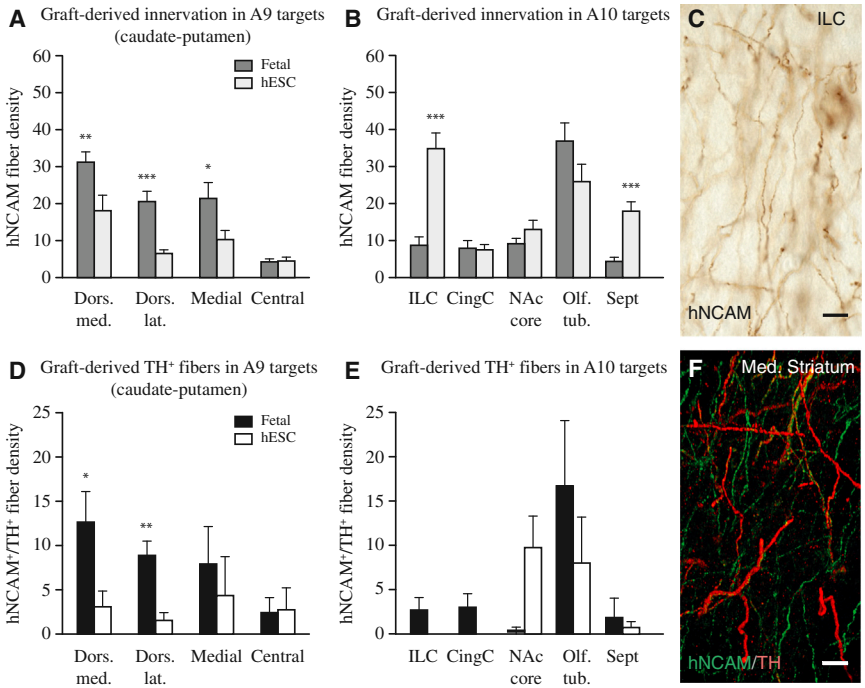

Figure 6. Quantitative Analysis of Neuronal Fiber Density in A9 and A10 Target Structures Derived from Intranigral Grafts

(A) Fetal VM grafts showed greater affinity to A9 targets in caudate-putamen (dark gray bars; n = 4) than to hESC-DA neurons (light gray bars; n = 4).

(B) Fetal VM and hESC-DA neurons were equally capable of innervating A10 targets, including NAc, olfactory tubercle, and cingulate cortex, while infralimbic cortex and septum received denser innervation from hESC-DA neurons.

(C) Example of a fiber density measurement performed on hNCAM immunostained sections.

(D) Colabeling with TH and hNCAM showed that both fetal VM and hESC-DA neurons were able to innervate the caudate-putamen, although DA neurons derived from fetal VM showed a stronger preference for the dorsal caudate-putamen than those derived from hESCs.

(E) $TH^+/hNCAM^+$ fibers were observed in all A10 targets innervated by fetal VM transplants (black bars; n = 3). hESC-derived $TH^+/hNCAM^+$ fibers were dense in NAc and olfactory bulb, but absent in cortical areas (white bars; n = 4).

(F) Confocal image of $TH^+/hNCAM^+$ section used for quantification.

See also Figure S5. CingC., cingulate cortex; Dors. lat., dorsolateral; Dors. med., dorsomedial; ILC, infralimbic cortex; MFB, medial forebrain bundle; NAc core, nucleus accumbens, core; Olf. tub., olfactory tubercle; Sept, septum. In (A), (B), (D), and (E), data are represented as mean ± SEM. *p < 0.05; **p < 0.01; ***p < 0.0001. In (C) and (F), scale bars represent 10 μm.

DISCUSSION

In this study, we have performed a comprehensive preclinical validation of hESC-derived DA neurons that fully supports their functional efficacy and capacity for long-distance, target-specific reinnervation, predictive of their therapeutic potential.

Using imaging techniques previously used to assess graft function in patients (Kefalopoulou et al., 2014; Piccini et al., 1999), we demonstrate that hESC-DA neurons survive, mature, and restore DA neurotransmission in the denervated striatum for up to 6 months postgrafting. When compared side-by-side with their fetal counterparts, the hESC-DA neurons appear identical in terms of morphology and marker expression, supporting their authenticity and stable phenotype. Importantly, we have also performed an equipotency assay, establishing that the hESC-DA neurons can completely reverse motor asymmetry in the drug-induced rotation test in numbers more than 10-fold lower than previously used (Kirkeby et al., 2012a; Kriks et al., 2011) and at a dose, i.e., a threshold number, of around 1,000 surviving DA neurons, similar to that seen with human fetal VM tissue (Brundin et al., 1986; Rath et al., 2013). Knowing that the number of surviving fetal DA neurons in a transplanted patient needs to be at least 100,000 in order to achieve a good clinical outcome (Hagell and Brundin, 2001), the equipotency data presented here will be important for guiding cell dosage when designing the first-in-man trial with hESCs.

We show that midbrain-patterned hESCs transplanted homotopically to the SN exhibit the same remarkable ability as their fetal counterparts to project axons over long distances in the adult brain, providing highly specific and appropriate innervation of midbrain DA target structures in the forebrain (Isacson et al., 1995; Wictorin et al., 1992). Intriguingly, and of clinical importance, this extensive axonal outgrowth occurs in the adult brain. While other reports have previously described long-distance outgrowth from transplants of hESC-derived neurons, these studies have been performed in neonatal rats and mice (Denham et al., 2012; Espuny-Camacho et al., 2013) and have not used hESCs patterned toward a specific dopaminergic fate. The capacity of the hESC-DA neurons to reinnervate previously denervated forebrain targets when transplanted to the SN is unparalleled and matched well the axonal outgrowth patterns obtained from grafts of authentic human fetal midbrain DA neurons.

Clinical studies show that grafts of fetal VM-derived DA neurons, transplanted to the DA-deficient putamen, can restore DA neurotransmission and provide functional benefits that are sustained over many years (Barker et al., 2013; Kefalopoulou et al., 2014). From preclinical studies we know that the efficacy of intrastriatal DA neuron grafts depends not only on the number of surviving DA neurons but also on their phenotype and their capacity to reinnervate a major part of the denervated target. We show here that the hESC-DA neurons generated by the current protocol are of the correct midbrain phenotype and contain the two major A9 and A10 DA neuron subtypes, similar to fetal VM grafts. This phenotype provides the grafts with the capacity to reinnervate both striatal and extrastriatal midbrain DAergic target structures. Importantly, we show that hESC-DA neurons are functionally equipotent to fetal VM neurons when grafted to the striatum and their axonal growth capacity matches that achieved by fetal VM neurons when grafted to the striatum and the SN. Data from transplantation studies in rodents and human autopsy cases indicate that DA neurons from human fetal VM have the capacity to extend axons for up to 5–7 mm in the

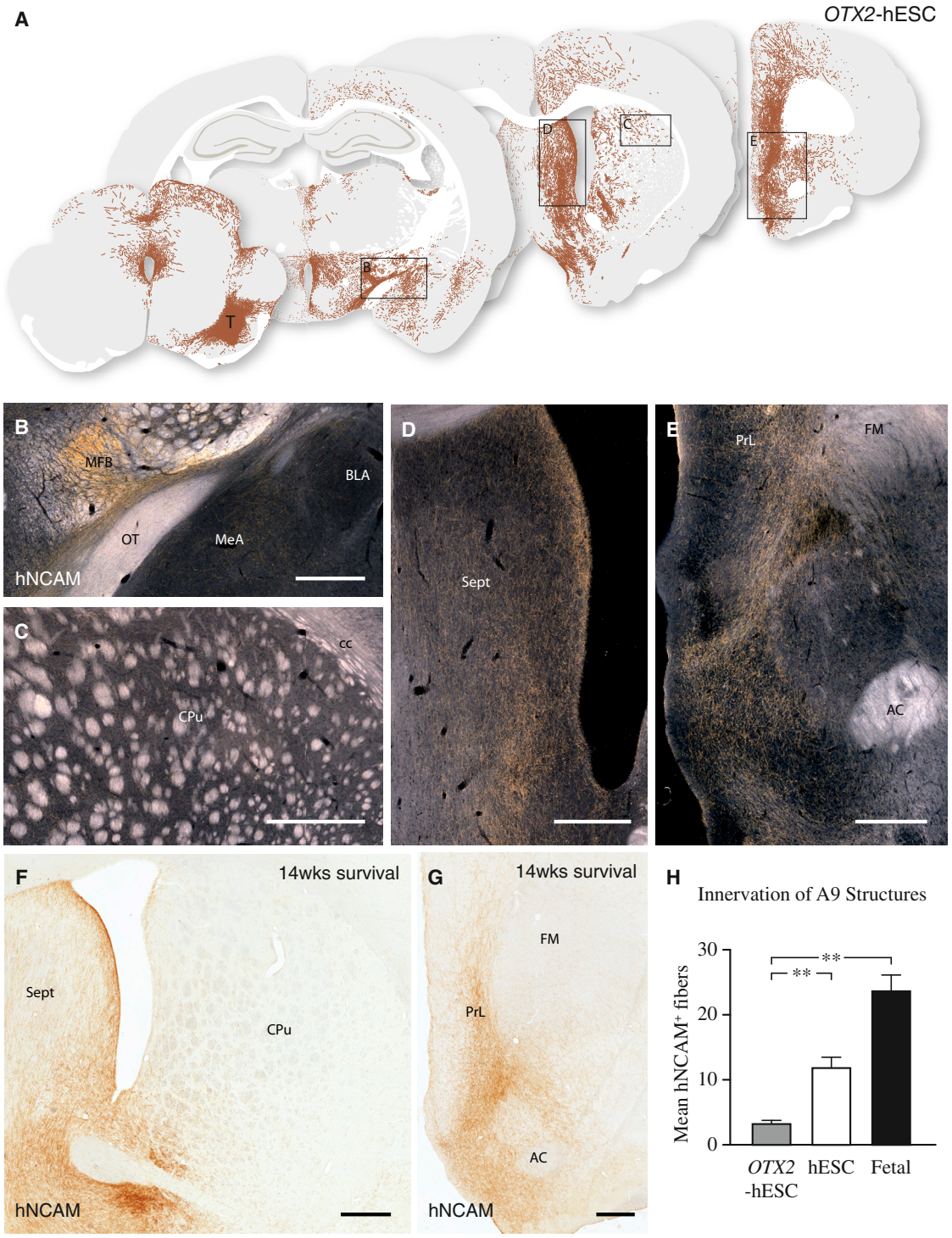

Figure 7. Maintained Expression of *OTX2* in hESC-Derived Neurons Results in an Altered Axonal Outgrowth Pattern

(A) Schematic overview of the pattern of hNCAM$^+$ axonal outgrowth derived from intranigral grafts of *OTX2*-hESCs 6 months posttransplantation, as visualized under dark-field illumination of DAB-developed sections (see Figure S6K). These cells displayed a strong preference for A10 target structures, such as septum, cingulate, prelimbic, and infralimbic cortices.

(B) The majority of axons extended rostral within the MFB, along both gray and white matter, with few axons innervating amygdala.

(C) Only rare hNCAM$^+$ axons were observed in caudate-putamen, the prime A9 target structure.

(D and E) Maintained expression of *OTX2* did not alter the long-distance growth capacity of the grafted neurons, as a dense fiber network was observed in both septum and NAc, as well as in prelimbic cortex.

(legend continued on next page)

striatum, which makes it possible to reinnervate a major part of the human putamen with a limited number of cell deposits (Freeman and Brundin, 2006; Kordower et al., 1995). The axonal outgrowth observed here, up to 10 mm from the graft deposit, indicates that the growth capacity of the hESC-derived DA neurons will be sufficient to provide efficient and widespread restoration of DA neurotransmission in the DA-denervated striatal targets in PD patients. The potency of the hESC-derived DA neurons, with respect to functional efficacy and long-distance targeted reinnervation, is on par with that of fetal VM cells, which provides important support for their therapeutic potential and use for cell replacement therapy in PD.

EXPERIMENTAL PROCEDURES

Research Animals

All procedures were conducted in accordance with the European Union Directive (2010/63/EU) and were approved by the ethical committee for the use of laboratory animals at Lund University and the Swedish Department of Agriculture (Jordbruksverket), as well as French legislation.

Athymic, nude rats were housed in individual ventilated cages, under a 12 hr light/dark cycle with ad libitum access to sterile food and water. Sprague-Dawley rats were kept in similar conditions as above, but in standard cages.

Experimental Design for Functional Imaging Experiment

Adult (<1 year) male, athymic, nude rats (Crl:NIH-*Foxn1*^{rnu}) were purchased from Charles River and used as graft recipients in all experiments and controls (n = 20). All rats received a 6-hydroxydopamine lesion of the medial forebrain bundle and 2 weeks later were assessed for lesion efficacy using amphetamine-induced rotations. All animals received longitudinal follow using MRI. The animals were stratified to the follow groups: baseline PET scanning, with subsequent follow-up scans at 5 to 6 months posttransplantation (n = 14), and MR spectroscopy of the grafts (n = 9).

Experimental Design for Circuit Reconstruction and Equipotency Experiments

Adult (<180 g) female, athymic, nude rats (Hsd:RH-*Foxn1*^{rnu}) were purchased from Harlan Laboratories and used as graft recipients and controls (n = 51). For repetition of the OTX2-overexpression and equipotency experiments, female Sprague-Dawley rats (225–250 g) were purchased from Charles River (n = 14 and n = 5, respectively). All surgical procedures, such as anesthetic doses, etc., were performed as described in detail (Grealish et al., 2010).

All rats received a 6-hydroxydopamine lesion of the medial forebrain bundle and 2 weeks later were assessed for lesion efficacy using amphetamine-induced rotations. The animals were stratified to the follow groups: intranigral grafting of fetal ventral mesencephalon (n = 8); intranigral grafting of hESC-derived DA neurons (n = 8); intranigral grafting of *OTX2*-hESCs, nude rats (n = 8), Sprague-Dawley rats (n = 14); equipotency intrastriatal grafting of hESC-derived DA neurons (n = 5); intrastriatal grafting of fetal tissue (n = 4); and lesion controls (n = 6).

Amphetamine-Induced Rotation

Rotational bias, after systemic amphetamine challenge (2.5 mg/kg, intraperitoneally; Apoteksbolaget), was recorded using an automated system (Omnitech Electronics). The animals were recorded for 90 min, and only full body turns were counted and then expressed as net turns per minute, with rotations toward the side of the lesion given a positive value. Only animals with more than 5 turns per minute were considered successfully lesioned.

Differentiation of hESCs

Human ESCs H9 (WA09, passages 31–45) were differentiated to a ventral midbrain fate, using the protocol as described in detail in Kirkeby et al. (2012b) and Supplemental Experimental Procedures.

Human Fetal Tissue

Human fetal tissue was obtained from legally terminated embryos with approval of the Swedish National Board of Health and Welfare in accordance with existing guidelines including informed consent from women seeking elective abortions. The gestational age of each embryo was determined by measuring the crown-to-rump length and/or estimated by ultrasound measurements. Embryos were then staged according to weeks postconception.

Transplantation Procedure

hESCs were prepared for transplantation as in Kirkeby et al. (2012a), while fetal tissue was prepared and transplanted as a semicrude suspension, as described in Rath et al. (2013).

Magnetic Resonance and PET Imaging

All specifications of these procedures are detailed in Supplemental Experimental Procedures.

Immunohistochemistry

All samples, cultured cells and brain tissue, were fixed in fresh 4% paraformaldehyde. A complete list of suppliers and concentrations of primary and secondary antibodies used is detailed in Supplemental Experimental Procedures.

Fiber Density Measurements

Quantitative analysis of the density of human fibers innervating specific areas was performed using a stereological method (Mouton et al., 2002). Details of sampling and acquisition are described in Supplemental Experimental Procedures.

Statistical Analysis

All data are presented as mean ± SEM.

Statistical tests and biological replicates are stated in results or in the figure legends. All statistical analyses were performed using GraphPad Prism v6.0 for Mac OS X. An alpha level of $p < 0.05$ was set as a threshold for significance.

In Figures 1B and 1C an unpaired t test was used to compare the baseline after 6-OHDA lesion and 5 months posttransplantation. In Figures 6A, 6B, and 6D, all fiber density was analyzed using a one-tailed unpaired t test. In Figure 7H the innervation of A9 structures in the *OTX2*-hESC group was compared with the hESCs and fetal VM grafted groups using a one-way ANOVA, with differences between groups confirmed using a Tukey's post hoc. The behavioral data in Figure 2A were analyzed with a two-tailed paired t test.

SUPPLEMENTAL INFORMATION

Supplemental information includes Supplemental Experimental Procedures and six figures and can be found with this article online at http://dx.doi.org/10.1016/j.stem.2014.09.017.

(F and G) In a repeat of this experiment in ciclosporin-treated rats, we confirmed that fiber outgrowth from *OTX2*-hESCs was confined almost exclusively to A10 target areas, such as NAc and septum (F) and prelimbic cortex (G). Notably, this outgrowth pattern was observed as early as 14 weeks after transplantation.
(H) *OTX2*-hESCs have a significantly impaired ability to extend hNCAM^{+} axons into A9 structures as compared with hESC and fetal grafts (all groups n = 3 animals with triplicate measures in four structures).
See also Figure S6. AC, anterior commissure; BLA, basolateral amygdala; CPu, caudate-putamen unit; FM, forceps minor; IC, internal capsule; MeA, medial amygdaloid nucleus; MFB, medial forebrain bundle; NAc, nucleus accumbens; OT, Olfactory Tract; PrL, prelimbic cortex; Sept, septum; T, transplant. In (H), data are represented as mean ± SEM. **$p < 0.001$
In (B)–(G), scale bars represent 0.5 mm.

ACKNOWLEDGMENTS

We would like to thank Jan Reimer, Olle Lindvall, and Jenny Nelander-Wahlestedt for acquisition and processing of human fetal material and Aurore Bugi for preparation and handling of hESC derivatives at I-Stem and Mircen. We would like to recognize the excellent technical assistance provided by Ulla Jarl, Michael Sparrenius, Anneli Josefsson, and Ingar Nilsson. The excellent technical support of Martine Guillermier in the PET imaging studies as well as the supply of PET radioligands by the radiochemistry unit of the Service Hospitalier Frédéric Joliot (directed by Frédéric Dollé) were very appreciated. This study was supported by grants from the European Community's 7th Framework Programme through NeuroStemcell (no. 222943), NeuroStemcellRepair (no. 602278), and TransEuro (HEALTH-F5-2010-242003); the strategic research area at Lund University Multipark (multidisciplinary research in Parkinson's disease); the Swedish Research Council (70862601/Bagadilico, K2012-99X-22324-01-5, and K2014-61X-20391-08-4); and the Swedish Parkinson Foundation (Parkinsonfonden). S.G. was supported by a postdoctoral stipend from the Swedish Brain Foundation (Hjärnfonden) and A.K. was supported via a grant from the Lundbeck foundation (R44-A3856). The research leading to these results has received funding from the European Research Council under the European Union's 7th Framework Programme (FP/2007-2013)/ERC Grant Agreement no. 309712.

Received: June 5, 2014
Revised: August 19, 2014
Accepted: September 24, 2014
Published: November 6, 2014

REFERENCES

Barker, R.A., Barrett, J., Mason, S.L., and Björklund, A. (2013). Fetal dopaminergic transplantation trials and the future of neural grafting in Parkinson's disease. Lancet Neurol. *12*, 84–91.

Barker, R.A. (2014). Developing Stem Cell Therapies for Parkinson's Disease: Waiting Until the Time is Right. Cell Stem Cell *15*, this issue, 539–542.

Brundin, P., Nilsson, O.G., Strecker, R.E., Lindvall, O., Astedt, B., and Björklund, A. (1986). Behavioural effects of human fetal dopamine neurons grafted in a rat model of Parkinson's disease. Exp. Brain Res. *65*, 235–240.

Chung, C.-Y., Seo, H., Sonntag, K.C., Brooks, A., Lin, L., and Isacson, O. (2005). Cell type-specific gene expression of midbrain dopaminergic neurons reveals molecules involved in their vulnerability and protection. Hum. Mol. Genet. *14*, 1709–1725.

Chung, C.-Y., Licznerski, P., Alavian, K.N., Simeone, A., Lin, Z., Martin, E., Vance, J., and Isacson, O. (2010). The transcription factor orthodenticle homeobox 2 influences axonal projections and vulnerability of midbrain dopaminergic neurons. Brain *133*, 2022–2031.

Denham, M., Parish, C.L., Leaw, B., Wright, J., Reid, C.A., Petrou, S., Dottori, M., and Thompson, L.H. (2012). Neurons derived from human embryonic stem cells extend long-distance axonal projections through growth along host white matter tracts after intra-cerebral transplantation. Front. Cell. Neurosci. *6*, 11.

Di Salvio, M., Di Giovannantonio, L.G., Acampora, D., Prosperi, R., Omodei, D., Prakash, N., Wurst, W., and Simeone, A. (2010a). Otx2 controls neuron subtype identity in ventral tegmental area and antagonizes vulnerability to MPTP. Nat. Neurosci. *13*, 1481–1488.

Di Salvio, M., Di Giovannantonio, L.G., Omodei, D., Acampora, D., and Simeone, A. (2010b). Otx2 expression is restricted to dopaminergic neurons of the ventral tegmental area in the adult brain. Int. J. Dev. Biol. *54*, 939–945.

Doi, D., Samata, B., Katsukawa, M., Kikuchi, T., Morizane, A., Ono, Y., Sekiguchi, K., Nakagawa, M., Parmar, M., and Takahashi, J. (2014). Isolation of human induced pluripotent stem cell-derived dopaminergic progenitors by cell sorting for successful transplantation. Stem Cell Rep. *2*, 337–350.

Dollé, F., Helfenbein, J., Hinnen, F., Mavel, S., Mincheva, Z., Saba, W., Schöllhorn Peyronneau, M.A., Valette, H., Garreau, L., Chalon, S., et al. (2007). One-step radiosynthesis of [18F]LBT-999: a selective radioligand for the visualization of the dopamine transporter with PET. J. Labelled Comp. Radiopharm. *50*, 716–723.

Espuny-Camacho, I., Michelsen, K.A., Gall, D., Linaro, D., Hasche, A., Bonnefont, J., Bali, C., Orduz, D., Bilheu, A., Herpoel, A., et al. (2013). Pyramidal neurons derived from human pluripotent stem cells integrate efficiently into mouse brain circuits in vivo. Neuron *77*, 440–456.

Freeman, T.B., and Brundin, P. (2006). Important aspects of surgical methodology for transplantation in Parkinson's disease. In Restorative Therapies in Parkinson's Disease, P. Brundin and C.W. Olanow, eds. (New York: Springer), pp. 131–165.

Gates, M.A., Olsson, M., Bjerregaard, K., and Björklund, A. (1998). Region-specific migration of embryonic glia grafted to the neonatal brain. Neuroscience *84*, 1013–1023.

Grealish, S., Jönsson, M.E., Li, M., Kirik, D., Björklund, A., and Thompson, L.H. (2010). The A9 dopamine neuron component in grafts of ventral mesencephalon is an important determinant for recovery of motor function in a rat model of Parkinson's disease. Brain *133*, 482–495.

Hagell, P., and Brundin, P. (2001). Cell survival and clinical outcome following intrastriatal transplantation in Parkinson disease. J. Neuropathol. Exp. Neurol. *60*, 741–752.

Isacson, O., Deacon, T.W., Pakzaban, P., Galpern, W.R., Dinsmore, J., and Burns, L.H. (1995). Transplanted xenogeneic neural cells in neurodegenerative disease models exhibit remarkable axonal target specificity and distinct growth patterns of glial and axonal fibres. Nat. Med. *1*, 1189–1194.

Kefalopoulou, Z., Politis, M., Piccini, P., Mencacci, N., Bhatia, K., Jahanshahi, M., Widner, H., Rehncrona, S., Brundin, P., Björklund, A., et al. (2014). Long-term clinical outcome of fetal cell transplantation for Parkinson disease: two case reports. JAMA Neurol. *71*, 83–87.

Kirkeby, A., Grealish, S., Wolf, D.A., Nelander, J., Wood, J., Lundblad, M., Lindvall, O., and Parmar, M. (2012a). Generation of regionally specified neural progenitors and functional neurons from human embryonic stem cells under defined conditions *1*, 703–714.

Kirkeby, A., Nelander, J., and Parmar, M. (2012b). Generating regionalized neuronal cells from pluripotency, a step-by-step protocol. Front. Cell. Neurosci. *6*, 64.

Kordower, J.H., Freeman, T.B., Snow, B.J., Vingerhoets, F.J., Mufson, E.J., Sanberg, P.R., Hauser, R.A., Smith, D.A., Nauert, G.M., Perl, D.P., et al. (1995). Neuropathological evidence of graft survival and striatal reinnervation after the transplantation of fetal mesencephalic tissue in a patient with Parkinson's disease. N. Engl. J. Med. *332*, 1118–1124.

Kriks, S., Shim, J.-W., Piao, J., Ganat, Y.M., Wakeman, D.R., Xie, Z., Carrillo-Reid, L., Auyeung, G., Antonacci, C., Buch, A., et al. (2011). Dopamine neurons derived from human ES cells efficiently engraft in animal models of Parkinson's disease. Nature *480*, 547–551.

Kuhnast, B., Damont, A., Hinnen, F., Catarina, T., Demphel, S., Le Helleix, S., Coulon, C., Goutal, S., Gervais, P., and Dollé, F. (2012). [18F]DPA-714, [18F]PBR111 and [18F]FEDAA1106-selective radioligands for imaging TSPO 18 kDa with PET: automated radiosynthesis on a TRACERLAb FX-FN synthesizer and quality controls. Appl. Radiat. Isot. *70*, 489–497.

Lindvall, O., and Kokaia, Z. (2009). Prospects of stem cell therapy for replacing dopamine neurons in Parkinson's disease. Trends Pharmacol. Sci. *30*, 260–267.

Mendez, I., Sanchez-Pernaute, R., Cooper, O., Viñuela, A., Ferrari, D., Björklund, L., Dagher, A., and Isacson, O. (2005). Cell type analysis of functional fetal dopamine cell suspension transplants in the striatum and substantia nigra of patients with Parkinson's disease. Brain *128*, 1498–1510.

Moon, B.S., Park, J.H., Lee, H.J., Kim, J.S., Kil, H.S., Lee, B.S., Chi, D.Y., Lee, B.C., Kim, Y.K., and Kim, S.E. (2010). Highly efficient production of [(18)F]fallypride using small amounts of base concentration. Appl. Radiat. Isot. *68*, 2279–2284.

Mouton, P.R., Gokhale, A.M., Ward, N.L., and West, M.J. (2002). Stereological length estimation using spherical probes. J. Microsc. *206*, 54–64.

Piccini, P., Brooks, D.J., Björklund, A., Gunn, R.N., Grasby, P.M., Rimoldi, O., Brundin, P., Hagell, P., Rehncrona, S., Widner, H., and Lindvall, O. (1999). Dopamine release from nigral transplants visualized in vivo in a Parkinson's patient. Nat. Neurosci. *2*, 1137–1140.

Piccini, P., Lindvall, O., Björklund, A., Brundin, P., Hagell, P., Ceravolo, R., Oertel, W., Quinn, N., Samuel, M., Rehncrona, S., et al. (2000). Delayed recovery of movement-related cortical function in Parkinson's disease after striatal dopaminergic grafts. Ann. Neurol. *48*, 689–695.

Pundt, L.L., Kondoh, T., and Low, W.C. (1995). The fate of human glial cells following transplantation in normal rodents and rodent models of neurodegenerative disease. Brain Res. *695*, 25–36.

Rath, A., Klein, A., Papazoglou, A., Pruszak, J., Garcia, J., Krause, M., Maciaczyk, J., Dunnett, S.B., and Nikkhah, G. (2013). Survival and functional restoration of human fetal ventral mesencephalon following transplantation in a rat model of Parkinson's disease. Cell Transplant. *22*, 1281–1293.

Reyes, S., Fu, Y., Double, K., Thompson, L., Kirik, D., Paxinos, G., and Halliday, G.M. (2012). GIRK2 expression in dopamine neurons of the substantia nigra and ventral tegmental area. J. Comp. Neurol. *520*, 2591–2607.

Ryan, S.D., Dolatabadi, N., Chan, S.F., Zhang, X., Akhtar, M.W., Parker, J., Soldner, F., Sunico, C.R., Nagar, S., Talantova, M., et al. (2013). Isogenic human iPSC Parkinson's model shows nitrosative stress-induced dysfunction in MEF2-PGC1α transcription. Cell *155*, 1351–1364.

Sachdeva, R., Jönsson, M.E., Nelander, J., Kirkeby, A., Guibentif, C., Gentner, B., Naldini, L., Björklund, A., Parmar, M., and Jakobsson, J. (2010). Tracking differentiating neural progenitors in pluripotent cultures using microRNA-regulated lentiviral vectors. Proc. Natl. Acad. Sci. USA *107*, 11602–11607.

Thompson, L., Barraud, P., Andersson, E., Kirik, D., and Björklund, A. (2005). Identification of dopaminergic neurons of nigral and ventral tegmental area subtypes in grafts of fetal ventral mesencephalon based on cell morphology, protein expression, and efferent projections. J. Neurosci. *25*, 6467–6477.

Wictorin, K., Brundin, P., Sauer, H., Lindvall, O., and Björklund, A. (1992). Long distance directed axonal growth from human dopaminergic mesencephalic neuroblasts implanted along the nigrostriatal pathway in 6-hydroxydopamine lesioned adult rats. J. Comp. Neurol. *323*, 475–494.

Cell Stem Cell, Volume *15*
Supplemental Information

Human ESC-Derived Dopamine Neurons Show Similar Preclinical Efficacy and Potency to Fetal Neurons when Grafted in a Rat Model of Parkinson's Disease

Shane Grealish, Elsa Diguet, Agnete Kirkeby, Bengt Mattsson, Andreas Heuer, Yann Bramoulle, Nadja Van Camp, Anselme L. Perrier, Philippe Hantraye, Anders Björklund, and Malin Parmar

SUPPLEMENTAL INFORMATION

Supplemental information includes 6 figures, detailed Supplemental Experimental Procedures and Supplemental References.

Figure S1

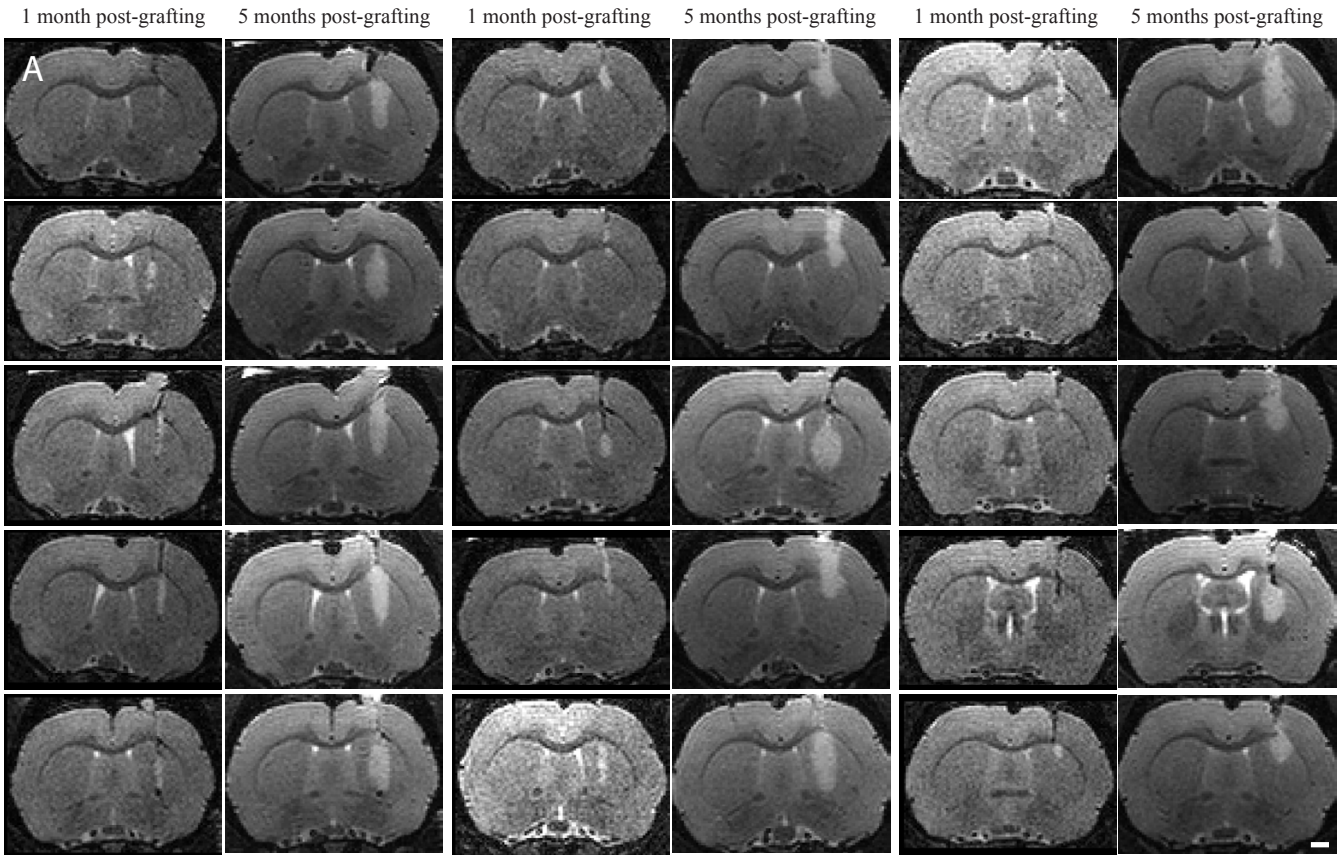

B

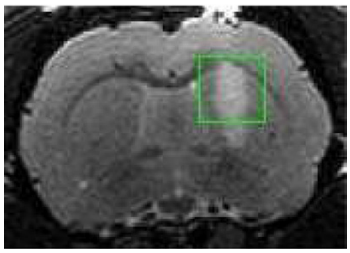

Voxel: 3x3x3mm^3

C

MRS 5M post-transplantation

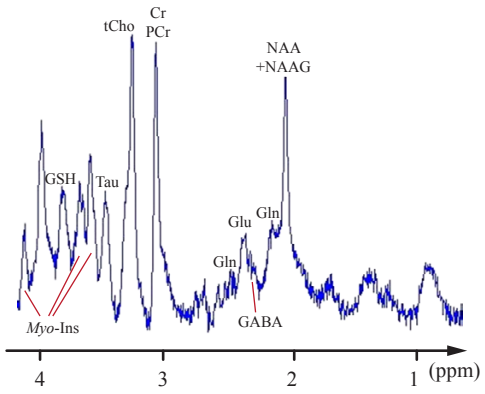

Figure S1 – Related to Figure 1

MRI scans and MR spectroscopy profile of long-term intrastriatal transplants of hESC-DA neurons.

(**A**) MRI scans for each individual animal (n=15) 1 and 5 months post-transplantation reveals well-placed transplants within the striatum that matured and occupied a larger volume over time, in the absence of any gross morphological damage or overgrowth formation. (**B**) Coronal view of the rat brain at the level of the graft, visualized by T2-weighted MRI. The green box delineates the area in which spectra were acquired. (**C**) A typical ^{1}H NMR spectra acquired *in vivo* in the area of the graft. In addition to commonly detected *N*-acetylaspartic acid (NAA, neuronal marker), creatine/phospho-creatine (Cr/PCr) and choline-containing compounds (tCho, membrane turnover marker), short echo-time detection allowed to visualize the presence of glutamate (Glu), Inositol (Myo-Ins, glial marker), taurine (Tau), glutamine (Gln), GABA, GSH (glutathione) within and around the graft, indicative of a normal profile of neurochemical metabolites.

Figure S2

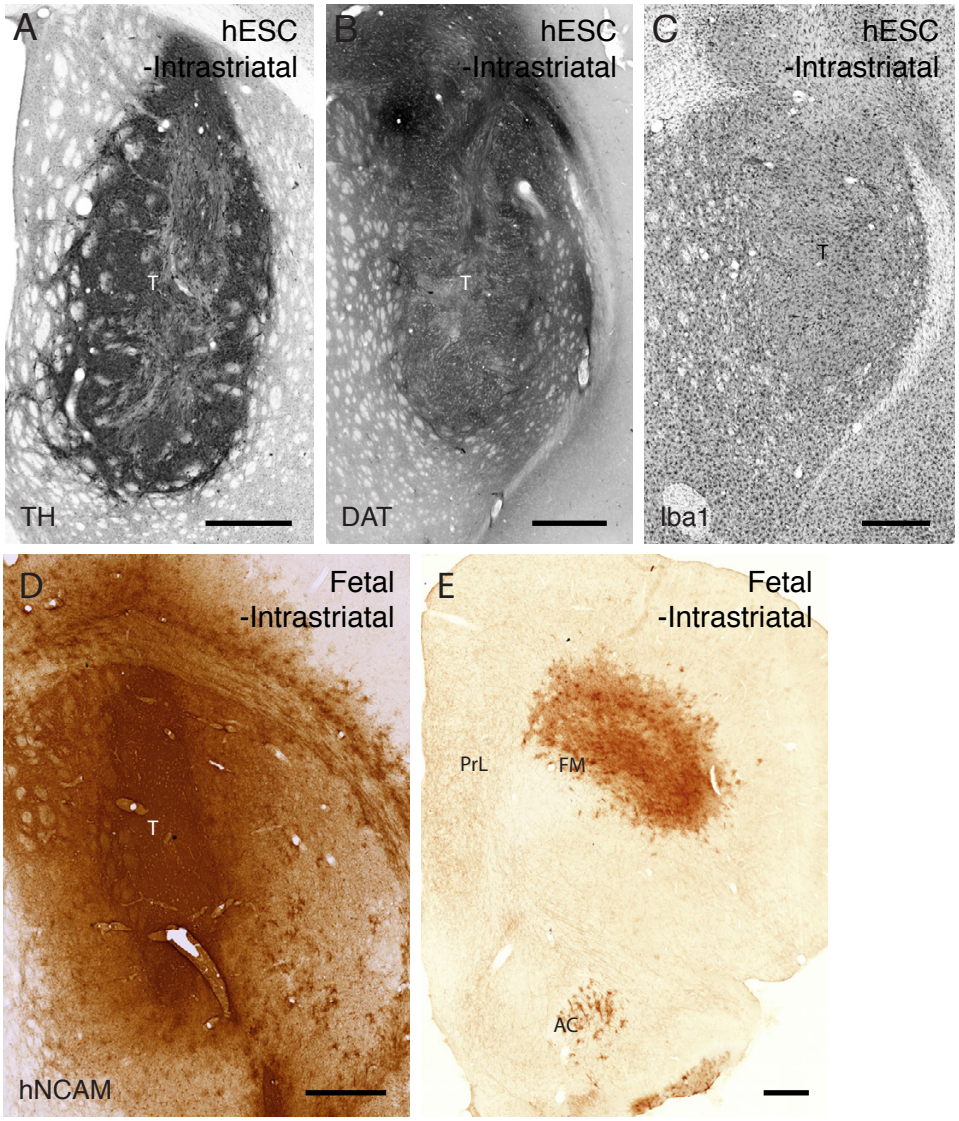
A
hESC
-Intrastriatal
T
TH
B
hESC
-Intrastriatal
T
DAT
C
hESC
-Intrastriatal
T
Iba1
D
Fetal
-Intrastriatal
T
hNCAM
E
Fetal
-Intrastriatal
PrL
FM
AC

Figure S2 – Related to Figure 2

Immunohistochemical analysis of intrastriatal transplants after 6 months survival.

Long-term intrastriatal transplants of hESC-DA neurons that underwent PET imaging contained a large numbers of surviving TH^+ neurons (**A**), and high dopamine transporter DAT levels (**B**), in the absence of any detectable immune response within or surrounding the graft core, as assessed by immunostaining for $Iba1^+$, a marker for activated microglia (**C**). (**D**) Immunostaining for hNCAM of fetal VM grafted to the striatum revealed a large, neuron-rich graft core that provided extensive innervation of the surrounding striatum, as well as being encompassed by a substantial number of $hNCAM^+$ glial cells. (**E**) Graft-derived $hNCAM^+$ fibers could be traced also outside the striatum, innervating areas of the prefrontal cortex, including the prelimbic cortex. A notable observation is the high number of glia migrating along the forceps minor, as shown in (**E**).

AC= anterior commissure; cc= corpus callosum; FM=forceps minor; PrL= prelimbic cortex; T=transplant.

Scale bars: **A-E** = 0.5 mm.

Figure S3


A
Fetal 8 w p.c.
T
hNCAM
B
Fetal 5.5 w p.c.
T
hNCAM
C
Fetal 5.5 w p.c.
IC
MFB
hNCAM
D
Fetal 5.5 w p.c.
MeA
BLA
E
Fetal 5.5 w p.c.
CC
CPu
F
Fetal 5.5 w p.c.
AC
NAc
G
Fetal 5.5 w p.c.
FM
PrL

Figure S3 – Related to Figure 4

Overview of intranigral transplants of fetal VM, 6 months post-transplantation.

(**A, B**) Coronal sections immunostained for hNCAM and visualized under dark-field illumination from intranigral transplants of fetal VM obtained from an 8-week (**A**) and a 5.5-week (**B**) donor. The images in (**A**) were used to generate the schematic in **Figure 4A**. (**C**) Inspection of the MFB revealed that $hNCAM^{+}$ fibers readily course through both gray and white matter. (**D**) Axons exit the MFB laterally to innervate nuclei of the amygdala. (**E**) $hNCAM^{+}$ axons from fetal VM sourced from the 5.5-week donor exhibited a strong preference for the dorsolateral caudate-putamen, as observed with grafts of 8-week VM. (**F**) Specific innervation of A10 target structures, such as NAc. (**G**) Long-distance axonal outgrowth was observed providing innervation of A10 cortical target structures, like prelimbic cortex.

AC= anterior commissure; BLA= basolateral amygdala; CPu= caudate-putamen unit; FM= forceps minor; IC= internal capsule; MeA= medial amygdaloid nucleus; MFB= medial forebrain bundle; NAc= nucleus accumbens; PrL= prelimbic cortex, T= transplant.

Scale bars: **A** and **B** = 1 mm; **C** = 100 μm, **D-G** = 0.5 mm.

Figure S4

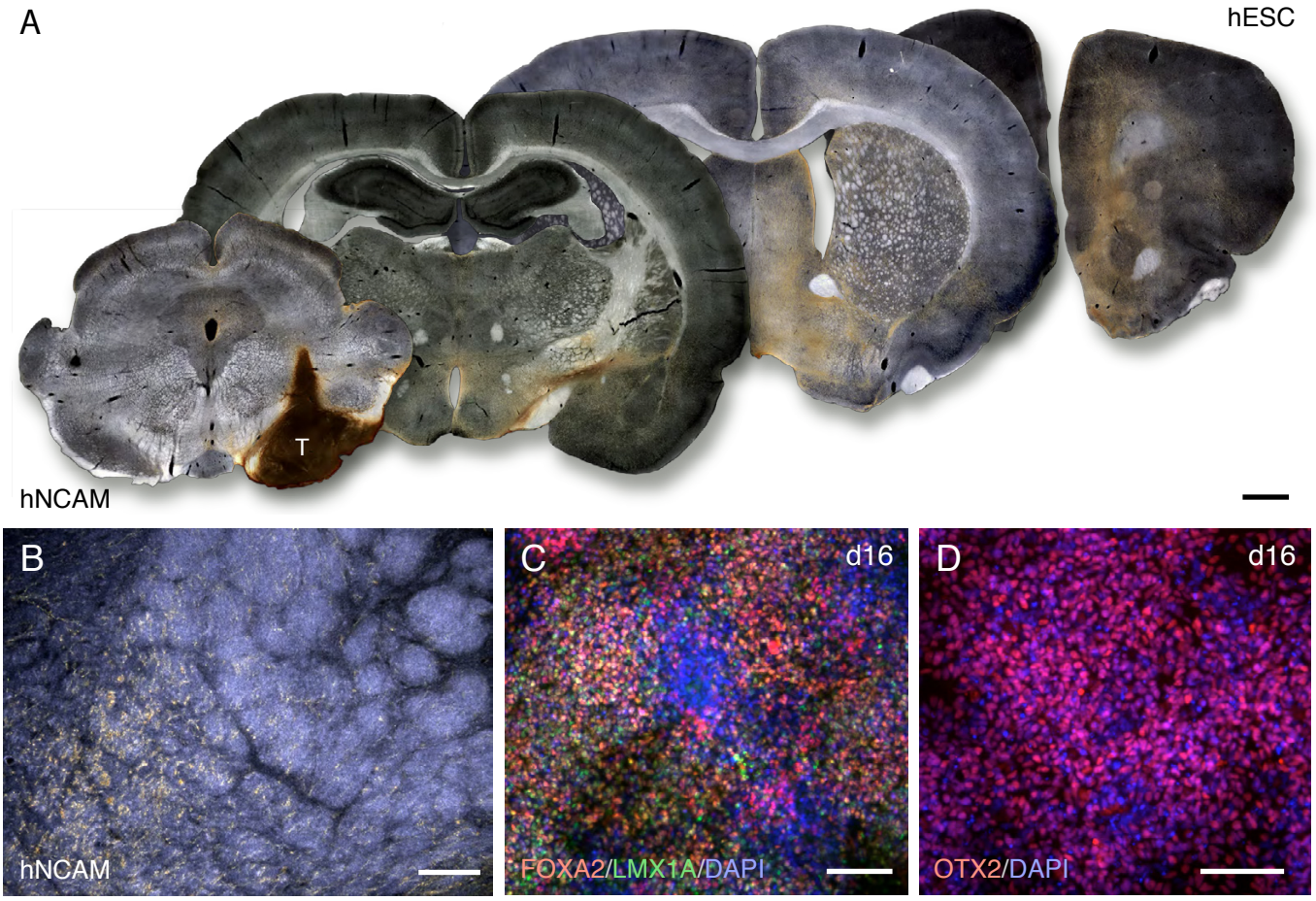

Figure S4 – Related to Figure 5

Overview of intranigral grafted hESC-DA neurons, 6 months survival.

(**A**) Dark-field images of the coronal sections used to generate the schematic in **Figure 5A** showing graft-derived outgrowth visualized using hNCAM immunohistochemistry. (**B**) Close examination of the MFB revealed that $hNCAM^{+}$ fibers coursed through both gray matter and white matter tracts, such as internal capsule. (**C, D**) *In vitro*, the cells used for transplantation, obtained from day 16 of hESC-differentiation, revealed a high co-expression of the midbrain DA progenitor markers FOXA2 and LMX1A (**C**), as well as a high proportion of OTX2 expressing progenitors (**D**).

Scale bars: **A** = 1 mm; **B-D** = 100 μm.

Figure S5

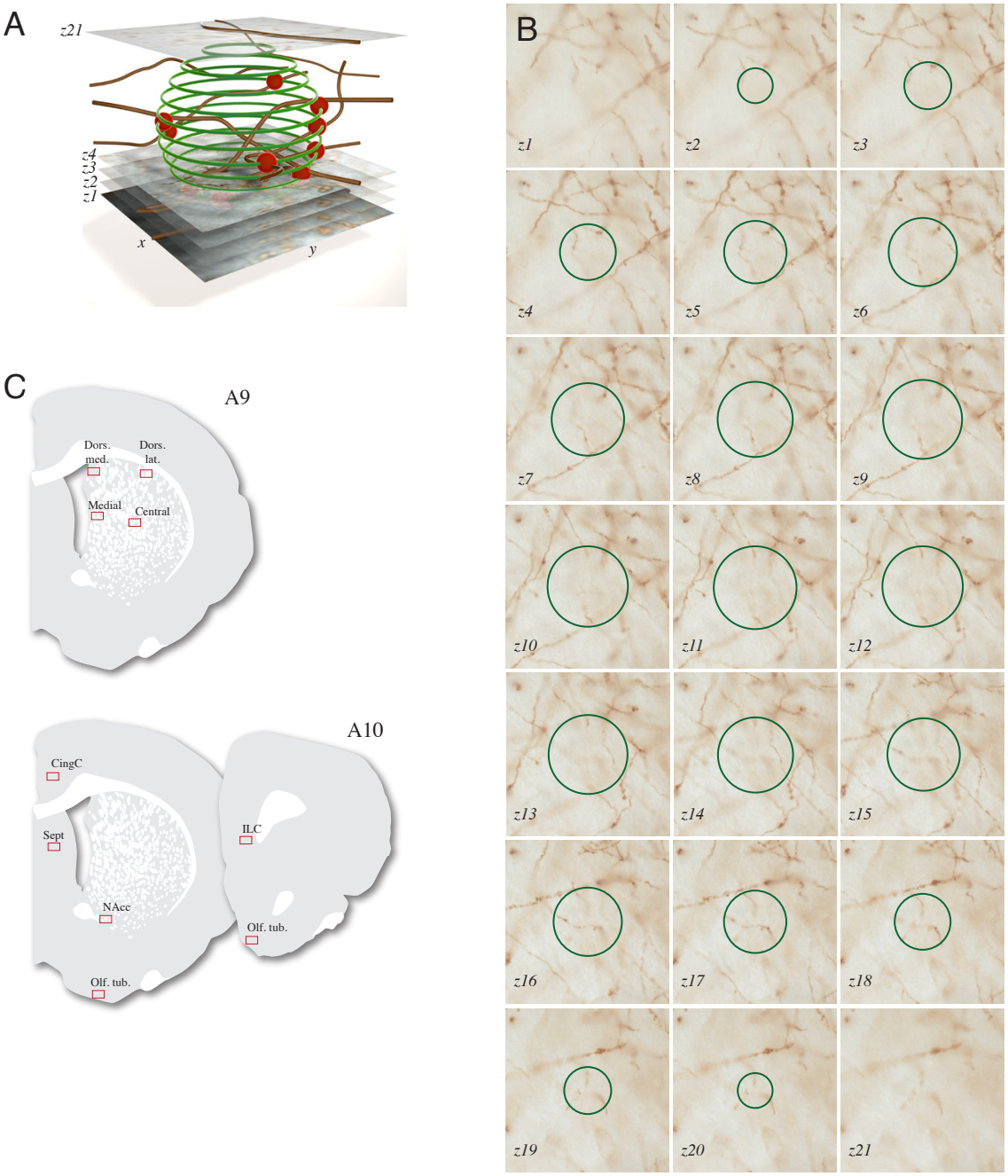
A
z21
z4
z3
z2
z1
x
y
B
z1
z2
z3
z4
z5
z6
z7
z8
z9
z10
z11
z12
z13
z14
z15
z16
z17
z18
z19
z20
z21
C
A9
Dors. med.
Dors. lat.
Medial
Central
A10
CingC
Sept
NAcc
Olf. tub.
ILC
Olf. tub.

Figure S5 – Related to Figure 6

Method used for fiber density measurements in A9 and A10 target structures.

(**A**) "Sphere method" for estimation of the number of fibers passing through a given volume. A z-stack through the whole section is taken at 1µm intervals, after which a sphere with a diameter of 19 µm is placed in. When a given fiber penetrates any edge of the sphere, a score of 1 is assigned. (**B**) Illustrative example of DAB-developed hNCAM staining at each level of the z-stack, with its respective outline of the measuring sphere. (**C**) Location of the A9 and A10 target structures from which z-stacks were obtained for quantitative analysis of either hNCAM (**Figures 6A, 6B** and **Figure 7H**), or TH^+/$hNCAM^+$ fiber density (**Figures 6D** and **6E**).

Central = central CPu; Cing. C. = cingulate cortex; Dors. lat. = dorsolateral CPu; Dors. med. = dorsomedial CPu; ILC= infralimbic cortex; MFB = medial forebrain bundle; NAc core= core of the nucleus accumbens; Olf. tub. = olfactory tubercle; Sept. = septum.

Figure S6

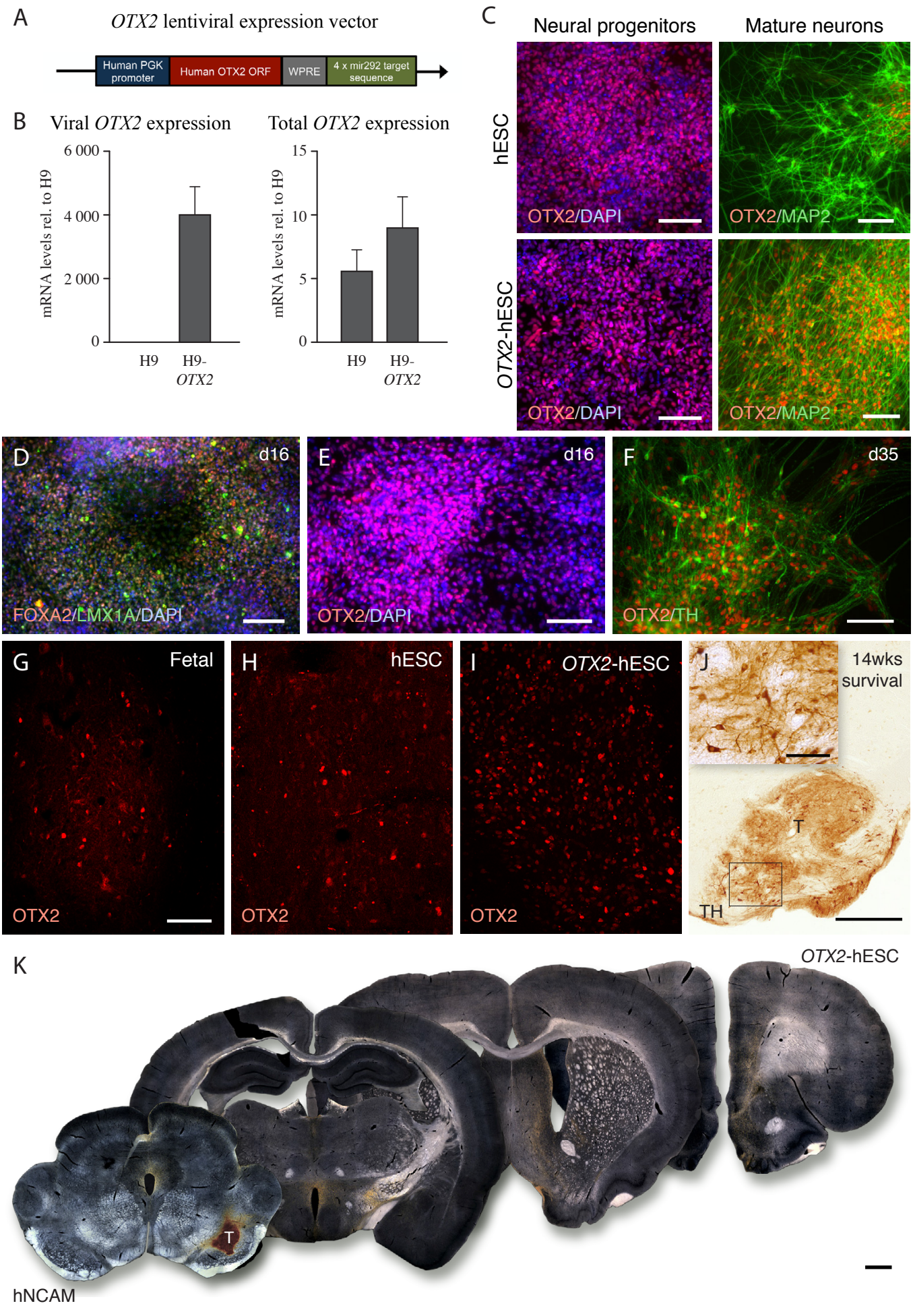
A
OTX2 lentiviral expression vector
Human PGK promoter
Human OTX2 ORF
WPRE
4 x mir292 target sequence
B
Viral OTX2 expression
Total OTX2 expression
mRNA levels rel. to H9
6 000
4 000
2 000
0
15
10
5
H9
H9-OTX2
C
Neural progenitors
Mature neurons
hESC
OTX2-hESC
OTX2/DAPI
OTX2/MAP2
D
d16
FOXA2/LMX1A/DAPI
E
d16
OTX2/DAPI
F
d35
OTX2/TH
G
Fetal
OTX2
H
hESC
OTX2
I
OTX2-hESC
OTX2
J
14wks survival
T
TH
K
OTX2-hESC
T
hNCAM

Figure S6 – Related to Figure 7

Overview of intranigral grafts of *OTX2*-hESCs, 6 months survival.

(**A**) A schematic of the lentiviral construct used for transgenic expression of *OTX2*. To ensure expression of the OTX2 protein only in differentiated cell populations, the vector was regulated by the pluripotency-specific microRNA, mir292, through the presence of 4 target sequences for mir292 in the 3' UTR of the mRNA. WPRE = Woodchuck hepatitis virus post-transcriptional regulatory element. (**B**) Quantitative RT-PCR was performed on differentiated cells (d16) to verify active transcription of the viral construct. It was further confirmed that total levels of *OTX2* mRNA were not significantly increased in transgenic cells compared to control midbrain-patterned hESC progenitors. (**C**) A differentiation experiment comparing hESCs and *OTX2*-hESCs revealed similar numbers of OTX2-expressing progenitors patterned to a midbrain fate. When allowed to terminally differentiate *in vitro* hESCs were seen to down-regulate OTX2 expression in mature neurons (as assessed by $MAP2^+$ cells), while the transgenic expression construct maintained a high level of protein expression at the same stage (d35). *In vitro* characterization of the *OTX2*-hESCs on the day of transplantation (d16) revealed a midbrain phenotype, as determined by FOXA2 and LMX1A co-expression (**D**), as well as an increase in the number of OTX2-expressing progenitors present within the cultures at the time of grafting (**E**) (compare with **Figure S4D**). (**F**) Long-term culture (d35) revealed that OTX2 over-expression is maintained in mature neurons, and that the cells could differentiate into TH^+ neurons. (**G-I**) Intra-nigral grafts of fetal VM (**G**) and hESCs (**H**) contained only a small fraction of OTX2 expressing cells, whereas a high level of OTX2 protein (**I**) expression was maintained in the cells derived from *OTX2*-hESCs.

(**J**) Maintained expression of OTX2 in these transplants did not affect their ability to give rise to TH^+ neurons with mature morphology after 14 weeks post-transplantation. (**K**) Dark-field coronal sections stained for hNCAM used to generate the schematics in **Figure 7A**. **B** Data are represented as mean ± SEM.

Scale bars: **C-I** = 100 μm; **J** = 0.5 mm, inset in **J** = 100 μm; **K** = 1 mm.

SUPPLEMENTAL EXPERIMENTAL PROCEDURES

Culturing and differentiation of hESCs

Human ESCs H9 (WA09, passage 31–45) (Thomson et al., 1998) were maintained on gamma-irradiated mouse embryonic fibroblasts in DMEM/F12, 20% KSR, 0.05 mM 2-mercaptoethanol, 0.5% Pen/Strep and 10 ng/ml FGF-2 (R&DSystems). The cells were passaged once weekly with EDTA (0.5 mM). Differentiation was performed as described in detail in (Kirkeby et al., 2012b). Briefly, cells were differentiated in 10 μM SB431542 (Tocris), 100 ng/ml Noggin (R&D), 200 ng/ml SHH-C24II (R&D) and 0.8 μM CT99021 (Axon Medchem) from day 0-9 of differentiation, using an embryoid body suspension culture for the first 4 days of differentiation. Neural colonies were passaged with accutase on day 11 and kept in medium containing 20 ng/ml brain-derived neurotrophic factor (BDNF), 10 ng/ml glial cell line-derived neurotrophic factor (GDNF), 200 mM ascorbic acid from day 11 until day 16, when the cells were dissociated with accutase and resuspended in HBSS + 0.05% DNAse for transplantation. For *in vitro* terminal differentiation, db-cAMP (0.5 mM) and DAPT (1 μM) was added to the medium from day 14.

Lentiviral expression of OTX2 in hESCs

The open reading frame for human *OTX2* was cloned into a previously described 3rd generation lentiviral construct containing 4 target sites for the microRNA mir292 in the 3' UTR (Sachdeva et al., 2010). High-titer lentiviral particles were produced as described in (http://www.ncbi.nlm.nih.gov/pubmed/9765382), and hESCs were infected at a multiplicity of infection (MOI) of 1:50. The polyclonal OTX2-mirT292

cell line was assessed for transgene expression, and the cells were differentiated as described above.

Immunocytochemistry and qRT-PCR analysis of hESCs

Prior to transplantation, correct VM specification of the differentiated hESCs was verified through immunochemical staining for OTX2, LMX1A and FOXA2 (see antibody specifications below), as well as quantitative RT-PCR using a panel of neural markers as described in (Kirkeby et al., 2012a). For verification of transgenic *OTX2* expression, viral-specific primers were used: Fwd: TCCCATGACCTATACTCAGGCT Rev: CCACATAGCGTAAAAGGAGCA.

Surgical procedures

All rats received a 6-OHDA lesion of the MFB as described in (Kirik et al., 1998).

For intrastriatal transplants of hESCs, a single deposit of 150 000 cells was transplanted to the striatum in a volume of 2 µl, at a concentration of 75 000 cells/µl, to the following co-ordinates relative to bregma: A/P +0.8; M/L +3.0; D/V (from dura) -4.0; tooth bar -3.3. For intrastriatal transplantation of fetal cells a preparation of 2 VMs (6 and 7.5 week p.c.) was dissociated and made to a final volume of 80 µl. 12 µl of which was transplanted to the striatum at the following co-ordinates: A/P +1.2; M/L -2.6; D/V -5.0 (3 µl) and -4.0 (3µl); and A/P +0.5; M/L -3.0; D/V -5.0 (3 µl) and -4.0 (3µl); tooth bar -2.4.

For intranigral transplantation of hESCs, 100 000 cells were transplanted in a volume of 2 µl with a concentration of 50 000 cells/µl on day 16 of differentiation at the following co-ordinates relative to bregma: A/P -4.6; M/L -2.2; D/V -7.0; tooth bar -2.4. Fetal VM, from individual fetuses aged 5.5 or 8 weeks p.c., was dissociated in 20 µl and 1.5 µl per rat was transplanted to the same co-ordinates.

Magnetic resonance imaging

T2-weighted images were acquired for each individual animal using a fast spin-echo sequence with the following parameters: TE, 20 ms; TR, 7000 ms; field of view, 38.4 × 38.4 mm; matrix, 256 × 256; resulting in a 150 × 150 µm in-plane resolution; 38 coronal slices with 300 µm thickness; acquisition time of 12 min.

In vivo LASER spectra were acquired from a single voxel spectroscopy (VOI, 3x3x3=27mm^3) centered within striatal graft. The placement of the MR spectroscopy volume of interest (square box) was determined using coronal T2-weighted images. All 1H-MRS spectra were obtained from the grafted striatum. The prominent peaks of biological importance in our study were those of the neuron-specific compound (NAA+NAAG), the Choline-containing compounds tCho (GPC+PCho) and myo-inositol-containing compounds.

The LCModel fitting software (Stephen Provencher, Inc., Oakville, ON, Canada) was used to quantify the metabolites in the frequency domain, using the basis set as discussed previously (Pfeuffer et al., 1999).

MicroPET imaging

Magnetic resonance imaging (MRI) was performed on a horizontal bore 7T system (Varian-Agilent Technologies) equipped with a gradient coil reaching 600 mT/m (120 μs rise time), a radiofrequency birdcage 1H coil for transmission, and a four-channel surface receive coil (Rapid Biomedical). MRI was used to follow the growth of transplanted cells within 6-OHDA-lesioned striatum to perform MR spectroscopy within graft area and to define anatomical regions of interest (ROIs) through PET/MRI coregistration.

Unilateral 6-OHDA-denervated athymic nude rats were scanned on a Concorde Focus 220 camera (Siemens) dedicated to small-animal imaging with a spatial resolution of 1.35 mm full-width at half maximum. They were imaged before and 5-6 months after hESC transplantation using [18F]-Fallypride and [18F]-LBT999 as radioligands to study post and pre-synaptic DA neurotransmission, respectively. All grafted rats were imaged using the 18 kDa translocator protein (TSPO) specific ligand [18F]-DPA-714 before sacrifice in order to detect any microglial activation associated with graft transplantation.

All imaging experiments were performed on spontaneously breathing rats anesthetized by a gaseous mixture of 100% O2 and isoflurane (induction 4%; maintenance 1.5-2%). Body temperature was continuously monitored using a rectal temperature probe and maintained normothermic (37.5°C) using a feed-back coupled heating blanket (Blanket Control Unit, Harvard Apparatus Limited®, Edenbridge, Kent, UK). The breathing rate of the animals was visually inspected. The rat's head was fixed in flat-skull position using a stereotactic device. Although different

stereotactic devices were used for MRI and PET imaging, the rat's head was fixed in a similar position, allowing the co-registration of the different imaging modalities.

Concomitantly with a bolus injection of [18F]-Fallypride (~1mCi) or [18F]-LBT999 (~1mCi) via a 26-gauge catheter in the tail vein, a 120 min emission scan was performed with an energy window of 350–750 keV and a coincidence time window of 6 ns. The attenuation correction factors of the animal bed were measured using an external Cobalt-57 point source; whereas attenuation correction from the animal was calculated from the emission scans. Finally, the emission sinograms (i.e. each frame) were normalized, corrected for attenuation, scatter and radioactivity decay, and reconstructed using FORE and OSEM 2D (16 subsets and 4 iterations).

PET time frames collected were summed and manually coregistered to the T2-weighted MRI for each animal, using rigid transformations. Coaligned MR images were used to define ROI (left striatum = Intact; right striatum = lesioned+grafted), based on anatomical landmarks, using an in-house image processing software (Anatomist, visualization tool of BrainVISA, http://www.brainvisa.info). This process was performed by the same operator for all experiments. The mean activity concentration values in the left and right ROIs were calculated and used to obtain regional time activity curves (TACs). These curves were then normalized for injected dose and body weight and expressed as percentage standardized uptake values (SUV): %SUV = [100 × ROI values (Bq/ml)]/[(injected dose (mCi) × 37.106)/body weight (g)].

Immunohistochemistry

All rats received a terminal dose of anesthesia 60 mg/kg sodium pentobarbitone i.p. (Apoteksbolaget, Sweden), once animals were fully anesthetized they were trans-cardially perfused with 50 ml saline, followed by 250 ml ice-cold 4% paraformaldehyde. The brains were removed and post-fixed for 2 hours before being transferred to 25% sucrose in PBS. After 48 hours equilibration the brains were sectioned on a freezing microtome (Leica) at a thickness of 35 μm in a 1:8 series.

All immunohistochemistry was performed using free-floating sections that were incubated with primary antibodies overnight at room temperature, or over 48 hours at 4°C, in an incubation solution of 0.1 M phosphate buffered saline with potassium containing 5% normal serum (for the species specific to the secondary antibody) and 0.25% Triton X-100. Secondary antibodies were diluted in the same incubation solution as above for 1 hour at room temperature. Detection of the primary–secondary antibody complexes was achieved by peroxidase driven precipitation of di-amino-benzidine (DAB), or conjugation of a fluorophore (either directly to the secondary antibody or with a streptavidin–biotin amplification step where necessary). All stained sections were mounted on gelatin-coated microscope slides. DAB-developed sections were dehydrated in an ascending series of alcohols before clearing with xylene, and finally coverslipped using DPX mountant. Fluorescent immunostainings were coverslipped using polyvinyl alcohol-1,4-diazabicyclo[2.2.2]-octane (PVA—DABCO), and left to dry overnight.

All secondary antibodies, biotinylated or directly conjugated, were purchased from Vector Laboratories, and used at a concentration of 1:400. Primary antibodies and their respective species and concentrations were used as detailed: rabbit anti-

Calbindin$_{28KD}$ (1:1 000; Swant); rat anti-DAT (1:1 000; Chemicon MAB369); goat anti-FOXA2 (1:500; Santa Cruz M-20); goat anti-GIRK2 (1:200; Millipore ab65096); mouse anti-human NCAM (1:1 000; Santa Cruz Eric-1); rabbit anti-IBA1 (1:1 000; Wako); rabbit anti-LMX1A (1:5 000; Millipore ab10533); goat anti-OTX2 (1:2 000; Neuromics); mouse anti-tyrosine hydroxylase (1:5 000; Immunostar); rabbit anti-tyrosine hydroxylase (1:1 000; Millipore ab152).

Microscopy

All brightfield and darkfield images were captured using a Leica DMI6000B equipped with an automated stage. All fluorescent images we acquired using a TCS SP8 laser-scanning confocal.

Dopamine neuron cell counts

Using DAB-developed immunohistochemistry for TH, all animals in the equipotency experiment were analyzed to estimate the average number of surviving dopaminergic neurons within the graft. For every section of the graft in a given series, the upper and lower focal plane (using a 20x objective on a brightfield microscope) was captured and overlaid to avoid errors in counting the same cell twice. All TH^+ neurons within the graft core were counted and the total number per animal was corrected for the series number.

Dopamine neuron subtype cell counts

A z-stack for the full depth of penetration (>19 μm) was captured for an area covering the entire graft across two sections. From a triple stain, first all TH^+ neurons were quantified separately, then all TH^+ neurons co-expressing either $GIRK2^+$, $Calbindin^+$ or both markers were counted. To account for differences in graft volume between cell sources, quantifications were performed from a section at the beginning of the transplant and at the section occupying the largest area for a given animal. The counts represent the average number of neurons counted from 2 sections of transplants from three randomly selected animals per group.

Fiber density measurements

We adapted the technique described by Mouton and colleagues (Mouton et al., 2002) for quantifying the density of human fibers in a given volume, within a specific A9 or A10 target structure. For quantification of $hNCAM^+$ fiber density in DAB-developed sections, a z-stack was taken at intervals of 1 μm, using a 100x oil-immersion objective on a brightfield microscope (Olympus AX70), generating an image size of 175 μm X 135 μm. For quantification of $hNCAM^+$ and TH^+ fiber density a z-stack with step size of 1 μm was captured on confocal using a 63x water-immersion objective, generating an image size of 138 μm X 138 μm. A given stack was complied using an image analysis software, Velocity v 5.4.2 (Perkin Elmer). Here a sphere with a diameter of 19 μm was created to measure fiber density within the whole z-stack (see schematic in **Figure S5A**). Through the extent of the sphere, the points at which fibers pass through the circumference of the sphere at each z-level (**Figure S5B**). A score of one was given for each fiber crossing. For **Figures 6A, 6B**

and **7H** three, non-over-lapping spheres were analyzed in each stack. In **Figures 6D** and **6E**, one probe was analyzed in all channels (*i.e.* TH, hNCAM, and $TH^+/hNCAM^+$). For each probe the total number of fibers occupying the sphere was expressed as a measure of fiber density within the measured volume.

For fibers passing through the MFB, z-stacks were captured from DAB developed sections stained for hNCAM, that had an area of 23,000 μm^2. This was then corrected to the total area of the MFB for each coronal level at which a z-stack was captured form measurement (-2.92 mm rostral to bregma, Paxinos and Watson, 5^{th} edition).

The A9 and A10 anatomical structures measured are clearly defined in **Figure S5C**, in the coronal levels depicted at (+3.0 mm and +0.72 mm to bregma).

SUPPLEMENTAL REFERENCES

Kirik, D., Rosenblad, C., and Bjorklund, A. (1998). Characterization of behavioral and neurodegenerative changes following partial lesions of the nigrostriatal dopamine system induced by intrastriatal 6-hydroxydopamine in the rat. Experimental neurology *152*, 259-277.

Mouton, P.R., Gokhale, A.M., and Ward, N.L. (2002). Stereological length estimation using spherical probes. Journal of Microscopy.

Pfeuffer, J., Tkac, I., Provencher, S.W., and Gruetter, R. (1999). Toward an in vivo neurochemical profile: quantification of 18 metabolites in short-echo-time (1)H NMR spectra of the rat brain. Journal of magnetic resonance *141*, 104-120.

Thomson, J.A., Itskovitz-Eldor, J., Shapiro, S.S., Waknitz, M.A., Swiergiel, J.J., Marshall, V.S., and Jones, J.M. (1998). Embryonic stem cell lines derived from human blastocysts. Science *282*, 1145-1147.